Hindawi Publishing Corporation
Journal of Combustion
Volume 2011, Article ID 528126, 20 pages
doi:10.1155/2011/528126

Research Article

Experimental Study on Diesel Spray Characteristics and Autoignition Process

Özgür Oğuz Taşkiran and Metin Ergeneman

Automotive Division, Faculty of Mechanical Engineering, Istanbul Technical University, 34469 Maslak, Istanbul, Turkey

Correspondence should be addressed to Özgür Oğuz Taşkiran, taskiranoz@itu.edu.tr

Received 25 August 2010; Revised 22 December 2010; Accepted 10 January 2011

Academic Editor: Constantine D. Rakopoulos

The main goal of this study is to get the temporal and spatial spray evolution under diesel-like conditions and to investigate autoignition process of sprays which are injected from different nozzle geometries. A constant volume combustion chamber was manufactured and heated internally up to 825 K at 3.5 MPa for experiments. Macroscopic properties of diesel spray were recorded via a high-speed CCD camera by using shadowgraphy technique, and the images were analyzed by using a digital image processing program. To investigate the influence of nozzle geometry, 4 different types of divergent, straight, straight-rounded, convergent-rounded nozzles, were manufactured and used in both spray evolution and autoignition experiments. The internal geometry of the injector nozzles were obtained by using silicone mold method. The macroscopic properties of the nozzles are presented in the study. Ignition behaviour of different nozzle types was observed in terms of ignition delay time and ignition location. A commercial Diesel fuel, *n*-heptane, and a mixture of hexadecane-heptamethylnonane (CN65—cetane number 65) were used as fuels at ignition experiments. The similar macroscopic properties of different nozzles were searched for observing ignition time and ignition location differences. Though spray and ignition characteristics revealed very similar results, the dissimilarities are presented in the study.

1. Introduction

Measured spray characteristics are classified into two basic categories; the first one is macroscopic characteristics, which involve spray tip penetration, spray cone angle, and the derivatives of them [1–23], and the second one is microscopic characteristics, which involve droplet velocity, droplet distribution, droplet diameter distribution, air-fuel ratio distribution, and so forth [7, 10, 12, 13, 16, 24–32]. Macroscopic properties of diesel spray can be recorded and analyzed with lesser and cheaper laboratory equipments than the ones that microscopic properties require. In addition to this, macroscopic characterization is more reliable, since they are in bigger dimensions and easily detectable.

Spray tip penetration is most fundamental characterization among the others. The most cited spray tip penetration equations are the ones proposed by Wakuri et al. [19], Dent [20], and Hiroyasu and Arai [21], and there are many researchers used or enhanced their equations [1, 9, 18, 33]. These models based on known parameters of injection system and operating conditions, such as injection and ambient pressure, nozzle diameter, and so forth. Though all semiempirical equations of above-mentioned authors assume that spray velocity is constant at its initial interval, near-zone investigations showed that the spray velocity is not constant even for this short range [3, 9]. During the needle lift period, the flow effective orifice geometry changes and causes very rapid intrusion. Needle lift and injection rate experiments show that this rapid penetration period is about 50–150 μs long [9].

The manufacturing details of the nozzle geometry, like inlet rounding and conicity are important parameters since they have stimulating effect on cavitation. Today's diesel engines use higher injection pressures with the implementation of common rail injection systems. The nozzle flow at high-pressure ranges has more tendencies to form cavitation.

It is shown that the nozzle type and nozzle geometry (L/D ratio) have influence on fuel-air mixing process and cavitation [25, 34]. Numerical and experimental studies show that sharp inlet nozzles have greater axial velocities at the nozzle inlet, thus produce low static pressure regions (cavity) that may initiate cavitation when the pressure fall below the fuel vapor pressure. Nurick commented that cavitation might be seen even at the regions where cavity pressures larger than vapor pressure [35]. Rounding at the nozzle inlet geometry and nozzle conicity has reducing influence on cavitation. It is proposed by Nurick, that the flow does not cavitate when the ratio of rounding radius to the nozzle diameter (r/D) gets larger than 0.14 [35]. Though cavitation leads structural damages on the nozzle, recent studies suggest that cavitation improve the fuel atomization and fuel-mixing process [25, 34, 36]. The nozzle geometry and its cavitation tendency must be settled at nozzle characterization studies.

The entire struggle on spray mixing and characterization investigations is related to its autoignition and combustion process. Ignition delay period starts with the injection of fuel and consist physical and chemical delay periods until the autoignition occurs. The process of fuel atomization, evaporation, and mixing with air take place in physical delay period. Then, chemical reactions begin slowly and initiate autoignition. This period is called the chemical delay period. The total ignition delay period is generally expressed by Arrhenius-like equations. According to these different ignition delay equations, the effective parameters on ignition delay are ambient conditions and fuel injection pressures. There are many authors proposed different coefficients for ignition delay equations [37–40]. Some researchers add new parameters to the ignition delay equations such as, effect of injection pressure [40] and nozzle geometry [37]. It is known that ignition delay time gets shorter as ambient pressure, ambient temperature and ignition pressure increase.

The autoignition location of the diesel spray is also another important research point. Dec [41] combined his studies on diesel spray combustion and proposed a conceptual diesel spray model in 1997. His work changed the diesel autoignition understanding. He depicted that ignition occurs progressively at multiple points across the downstream regions of all the fuel jets, beginning well before the start of the premixed burn spike. In the next study of Dec and Espey [42], autoignition of diesel fuel was investigated. The chemiluminescence imaging results showed that the first detectable soot luminosity in isolated pockets occurs randomly along the sides of the liquid-fuel in the upstream portion of some of the fuel jets.

The nozzle geometry effect on spray development has been widely investigated in the literature. However, the connection between the nozzle geometry and ignition delay has not been extensively investigated yet. In this study, four nozzles were manufactured and their real inlet geometries were measured. As a first goal of this study, the connections of nozzle geometry and spray macroscopic properties will be presented. Second, ignition behavior of the manufactured nozzles will be presented. This study investigates and reveals whether the nozzles that have similar macroscopic properties, have similar autoignition behaviour, or not.

2. Theoretical Analyses

Nozzle discharge coefficient is a good parameter which helps to make a theoretical flow characterization of different nozzle types. The actual mass flow, m_f, is different from the theoretical ones because of friction and contraction of the flow inside the nozzle. The discharge coefficient, C_d, defines the ratio of actual and theoretical fuel flow:

$$C_d = \frac{\dot{m}_f}{\dot{m}_{\text{th}}} = \frac{\dot{m}_f}{A_0\sqrt{2 \cdot \rho_f \cdot \left(P_{\text{inj}} - P_{\text{back}}\right)}}, \tag{1}$$

$$\dot{m}_f = u_{\text{eff}} \cdot \rho_f \cdot A_{\text{eff}} = u_{\text{mean}} \cdot \rho_f \cdot A_0. \tag{2}$$

After the fuel injected into the chamber, spray penetration is defined as an important spray characteristic. In the literature, different researchers define this characteristic with one or two equations [1, 9, 18–21, 33]. Two equations for describing the spray penetration is more realistic. When the spray first injected into the chamber, the initial velocity of the spray tip is much larger than the surrounding air. According to Hiroyasu and Arai [21], at this zone the penetration is described by an expression proportional to time, t, in other words; it has constant velocity. At the next time step, when the spray velocity slows downs, the penetration at this zone is proportional to square root of time, $t^{0.5}$. Hiroyasu and Arai [21] describe the distinguishing time between these two time steps as breakup time:

$$S(t) = 0.39\sqrt{\frac{2\Delta P}{\rho_f}}t \quad \text{for } 0 < t < t_{\text{break}}, \tag{3}$$

$$S(t) = 2.95\left(\frac{\Delta P}{\rho_a}\right)^{1/4}\sqrt{d_0 t} \quad \text{for } t \geq t_{\text{break}}. \tag{4}$$

The second most attractive parameter is spray cone angle for spray characterization. Theoretical and experimental studies reported in the literature show that, spray angle is quasiconstant after spray developed enough and empirical equations describing the spray angle do not include a time variable. According to Hiroyasu and Arai [21] cone angle is as follows:

$$\theta = 83.5\left(\frac{l}{d_0}\right)^{-0.22}\left(\frac{d_0}{d_{\text{sack}}}\right)^{0.15}\left(\frac{\rho_a}{\rho_f}\right)^{0.26}. \tag{5}$$

Another important characterization parameter for spray development is its ignition delay. Related to defining ignition delay, different correlations which are based on temperature and pressure parameters can be found in the literature. Numerous correlations based on experimental data are in the form of Arrhenius equation, but the constants in correlations vary by several orders of magnitude [43–45]. The reason of this variety might be related to different experimental conditions. The most used form for defining the ignition delay is;

$$\tau = A \times P^{-n} \times e^{B/T}, \tag{6}$$

where τ is the ignition delay, A is a constant, P and T are the ambient gas pressure and temperature at the time

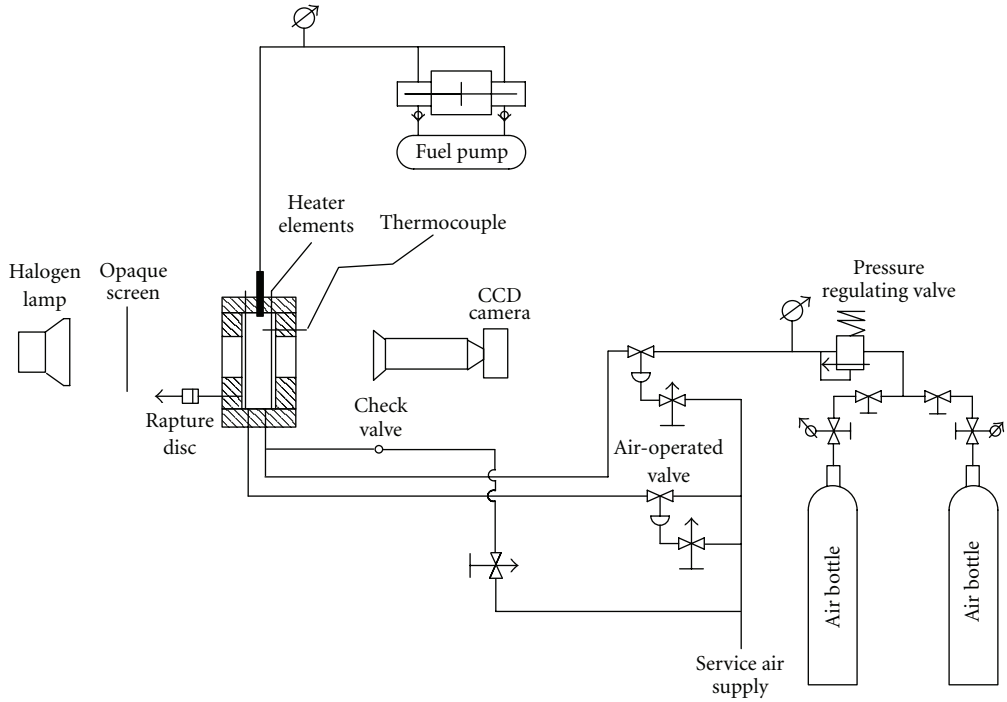

Figure 1: Schematic view of the experimental setup.

of autoignition [14, 39, 40, 44, 45]. Pischinger et al. [39] enhanced the basic equation by changing denominator of the superscripts T with $(T - T_0)$, where T_0 is defined as reference temperature that no ignition is observed. A reducing effect on ignition delay when injection pressure increased has been reported by Pischinger et al. [39]. The new equation constants proposed by Pischinger et al. [39] is as follows:

$$\tau = 6.97 \times P^{-1.14} \times e^{763.75/(T-T_0)}. \quad (7)$$

However, Pischinger's experiment was carried under a steady flow environment. The equation derived from constant volume experiment is needed in order to make a comparison between the experimental results with predicted ones. The equation constants proposed by Fujimoto is obtained from the constant volume experiments [46], and the equation proposed by Fujimoto is as follows:

$$\tau = 1.37 \times P^{-1.06} \times e^{5130/T}. \quad (8)$$

Since this equation is obtained from similar experimental setup with this study, it is expected to give similar results.

3. Experimental Setup and Experimental Technique

3.1. Constant Volume Combustion Chamber (CVCC). In this study a constant volume combustion chamber 56 mm in diameter, and 85 mm in depth and capable of heating the chamber air up to 850 K was designed and manufactured for spray experiments. Chamber interior wall is coated with a ceramic powder and resign mixture in order to insulate heater element. Heater element specially designed to heat the chamber homogeneously and not to affect spray periphery. It is manufactured from 0.5 mm thick stainless steel plate (Material Number: 1.4301, ANSI Code 304). The injector is mounted on to the center of top cover, thus spray periphery coincide with the chamber axis. The chamber equipped with two opposite 25 mm thick quartz windows which enable a 55 × 25 mm sight view of the chamber (spray) and a steel window which have j type thermocouple, safety head with burst disks and pressure gauge link on it. The air inlet and outlet pipes were mounted on the bottom cover and the injector holder was mounted on the upper cover which is cooled to prevent overheating of the injector. Compressed air supplied from two high-pressure (200 bar) air bottles via pressure reducers to obtain 2 and 3 MPa test conditions as shown in Figure 1. In addition, 0.6 MPa air supply is used both for low-pressure tests and also as auxiliary air to scavenge tested air-fuel mixture and combustion products. Air-operated inlet and outlet valves are capable of operating at 1000 K and 20 MPa.

The heater element voltage is supplied by a power supply unit which has output voltage range between 0–15 V and current range between 0–150 A. Temperature indicators mounted onto the power supply unit to observe the vessel temperature. A PDI control unit is also mounted inside the power supply unit to prevent the constant volume vessel overheated.

Before the experiments carried out, the temperature distribution inside the chamber were measured. Place-to-place temperature measurements showed that the points closer to the heater element had higher temperatures. However, when the chamber was heated up to 800°K, the

Table 1: Nozzle properties (manufacturer's data).

Nozzle	Q at 100 bar	*k-factor*	Hydrogrinding	Hole Dia. Ø mm
A	120 cm^3/30 s	−1.5	No	D_i : 0.225, D_o : 0.240
B	170 cm^3/30 s	0	Yes	0.240
C	170 cm^3/30 s	0	No	0.273
D	170 cm^3/30 s	+1.5	Yes	D_i : 0.255, D_o : 0.240

maximum temperature variation inside the chamber was 26°K, except the measurement points closer than 10 mm to heater.

Fuel control unit is a typical common rail-type system that consists of fuel tank, thermocouple, filter element, high-pressure pump driven by 3 KW electric motor, pressure regulating valve (DRV), pressure measurement sensor, high-pressure pipes as fuel accumulator (rail), solenoid-driven injector (Bosch P.N: 0445110146) and electronic fuel control unit specially designed for experiments. The electronic fuel control unit capable of producing injector signal, of which duration and requested injection pressure is given as input data before the experiment.

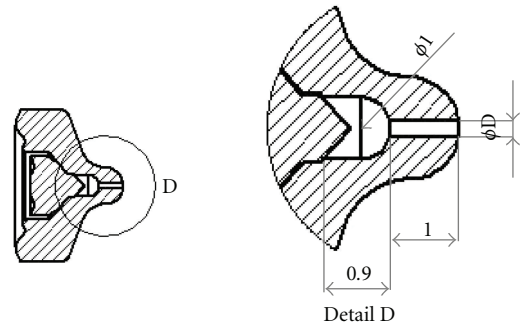

Figure 2: Specially manufactured nozzle dimensions.

3.2. Camera System. The cycle resolved images of the spray were obtained by FASTCAM 512-PCI Photron high-speed video camera system. In this study, the images were photographed by using 16000 fps with 512 × 64 and 32000 fps with 512 × 32 pixels resolutions. The time interval between the two recorded images is 31.25 μs or 62.5 which depends on chosen frame rate. The chosen exposure duration is equal to time interval because of the need of higher light intensity for lower exposure durations.

Since it is most fundamental and straightforward, observations on macroscopic spray characteristics; autoignition, autoignition sides and flame lift-off length has been carried out by using shadowgraphy technique [47]. The spray tip penetration data were obtained by using a digital imaging program which enables to use the same threshold level to distinguish spray tip from the background and also measure the distance between the nozzle hole and spray tip. A continuous 250 W light source, Dedocool lighting system and an opaque screen were used to obtain shadowgraph images of the spray. A more uniform distribution of the source light on the spray is obtained by using opaque screen placed between the light source and the back window. This opaque screen scatters nonuniform intensity illumination which is at its highest level in the center of the light beam and prevents overexposure which may lead misdetection of less dense, outer and weak edges of the spray shadow.

3.3. Nozzles and Their Dimensions. To investigate the effect of nozzle geometry, four nozzles were specially manufactured for experiments. Each nozzle has one hole coincided with the nozzle axis. Thus, the injected spray axis also coincide with the chamber axis. The schematic diagram of the injector nozzle is given in Figure 2 and the properties of the used nozzle types are given in Table 1. They are all have length/diameter ratio of ∼4. Hydrogrinding process was performed for Nozzle B and Nozzle D. The nozzle hole diameters are not identical in order to keep the same nozzle flow rate. Except Nozzle A, the flow rates of the nozzles, Q, defined as fuel rate injected at 100 bar are identical.

Conicity of the nozzles is represented by *k-factor*, which is a parameter indicating the diameter difference of inlet and outlet holes (it is defined as $k\text{-}factor = (D_i - D_o) \cdot 100$). Nozzle A has divergent shape and Nozzle D has convergent shape.

The real dimensions of the test nozzles were obtained by using Nikon LV 150 industrial microscope. Clemex Vision software program was used for microscopy image analysis. The magnified photos of the nozzle outlets are presented in Figure 3. There are little differences between the manufacturer's data and the measured dimensions. However, the outlet hole measurements may mislead the researcher since the tangent circle profile plotted on to the magnified photo does not perfectly fit into black circle area. Besides that, the nozzle outlet might have its natural rounding or chamfered shape. The real dimensions could be obtained by measuring the internal section diameter of the nozzle holes.

The procedure for the determination of internal geometry of nozzles is similar to the Macián et al. [48]. Polyvinylsiloxane which is a dental impression material is used for molding measurement experiments. This silicone consists of two pastes; a base (from silane group) and a catalyst (from vinyl group). These pastes are mixed together to produce a silicone rubber. There are many advantageous of this type of dental impressions materials such as; excellent dimensional stability, excellent elastic recovery, high tear strength, and availability.

The silicone mold was introduced into a sac volume via a plastic tube in order to reduce interior adherence. The tip of the plastic tube has screw teeth shape, so it grabs the silicone

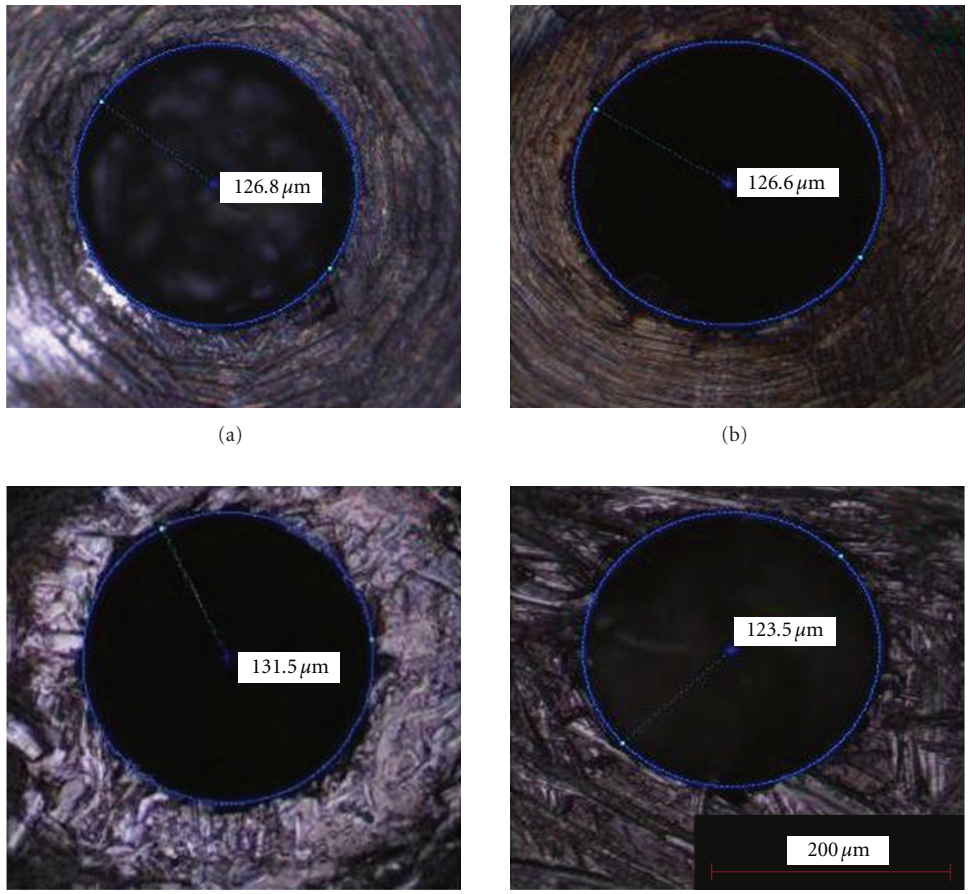

Figure 3: The nozzle outlet measurements with metallurgical microscope.

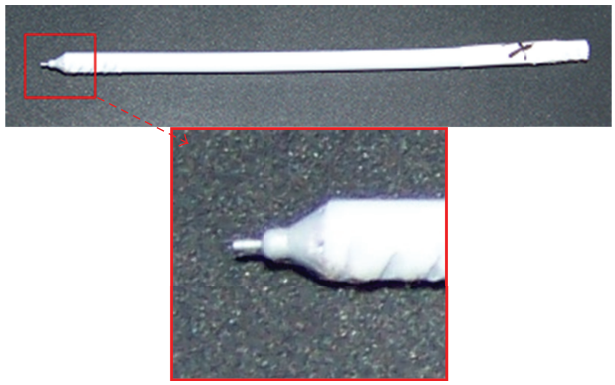

Figure 4: The plastic tube used in the silicone mold measurements.

mold better. The sac volume shape obtained from silicone mold at the tip of plastic tube could be seen in Figure 4.

The silicone mold were magnified and dimensioned in the microscope and magnified photos are presented in Figure 23. The results revealed that the inlet radius of the hydro-grinded nozzles do not have similar inlet radius (see Figure 23). The manufacturer's data suggests that Nozzle B and D have been exposed to hydro-grinding process. However, the results show that Nozzle B has approximately 120 μm and Nozzle D has approximately 50 μm inlet radius. The other dimensions obtained from the silicone mold measurements were very close to manufacturer's data. The maximum measured dimension difference is of $\pm 9\,\mu$m which may be attributed to manufacturing tolerances and measuring errors.

3.4. Fuels. Three kind of fuels have been used in the experiments; these were standard automotive diesel fuel (ADF), *n*-heptane (NH), and mixture of *n*-hexadecane and heptamethylnonane (CN65). The CN65 fuel was obtained by mixing 59% *n*-hexadecane and 41% heptamethylnonane (by volume). The fuel tank of the experimental setup was emptied and the remained fuel in the connection pipes was drained after completing experiments with one kind of fuel. However, there are always some residuals inside the pipes, injector, and high-pressure pump. These remainder fuel quantities may change the tested fuel. Thus, the used fuels have to be tested after completing the experiments in order to get real fuel properties.

The properties of fuels are presented in Table 2. Cetane index was calculated from empirical equation given in ASTM standard D 4737. This equation include T10, T50

Table 2: Fuel properties of the tested fuels.

Property	ADF	HN	CN65	Obtained from
Cetane number	55	56	65	Manufacturer's data
Cetane index	55	n.a	69	ASTM D 4737
Density (kg/m^3)	828.1	702.7	792.6	KEM DA-500 Density/Sp.Gra.
Viscosity (cst—40°C)	3.034	0.745	2.139	TANAKA AKV-202 Auto Kin.Vis.
Flash point °C	59	n.a	31	Petrotest Series 3
Water content (ppm)	56.3	69.2	22.5	Karl-Fischer MKC-501
H. heat value (joule/gr)	46478	46643	46958	IKA C 200 Bomb Calorimeter

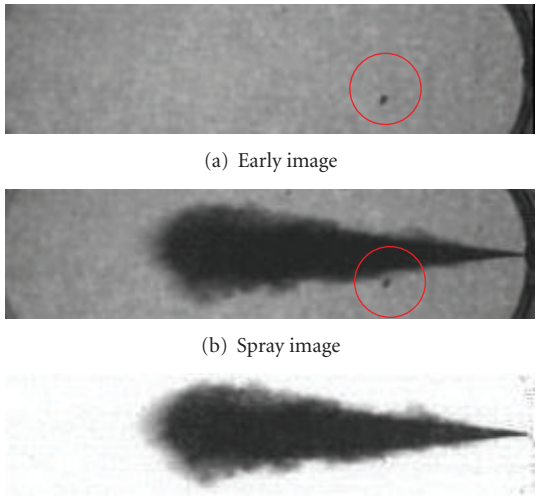

(a) Early image

(b) Spray image

(c) Corrected spray image

Figure 5: The illumination and fouling correction.

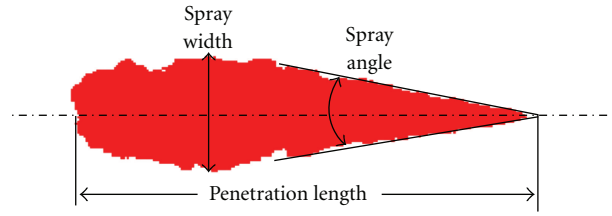

Figure 6: Measurement points of spray. Red color represents the spray projection area.

and T90 distillation temperatures and density as variables. The distillation temperatures of the fuels were obtained from TANAKA AD6-Auto Distillation Tester. The other test equipments are presented in Table 2.

3.5. Experimental Technique. Experiments on spray characteristic were carried mainly with diesel automotive fuel. Just to make a comparison, *n*-heptane was also used in spray characterization experiments. In order to see the difference of fuel type three different types of fuels were used for autoignition test. The experimental conditions are summarized in Table 3.

The illumination and fouling correction was carried out by using an early image of the experimental setup where no spray shadow was present. The spatial illumination and transmission of fouling on this early image was subtracted from the spray image. An example for the images that have window fouling and illumination nonuniformity is given in Figure 5. Before the correction, there is an ambiguity at determining the periphery of spray. However after correction, the resulted image is very clear and spray periphery is easily determined by image analyzing program.

If low frame rates are used, the injection delay time gets important in synchronizing the camera system with spray first images. The uncertainty gets lower when higher frame rates are used. In order to capture the initial stages of spray and reduce the uncertainty about the timing, high frame rates, 16000 and 32000 fps with continuous recording are used in this study. The corresponding time uncertainties are below 0.0625 and 0.03125 ms which are acceptable for spray evolution.

When the corrected images are obtained, the image geometries must be converted to the real geometries. Converting the measured distance into the real distance was calculated as follows: at first, a known distance between two points on the image was measured and a converting parameter was obtained. Then the measured distance of the spray was converted into actual distance.

The measurements were carried out by following the same procedure presented in Figure 6. In this paper, spray tip penetration length is measured from the injector tip to spray tip, which is defined as the intersection of the spray contour—determined by chosen threshold level—and spray axis. The spray cone angle measurement is obtained separately from the spray length measurements. It is measured between the tangent lines fitted through the upstream half of the spray contour. Besides penetration and cone angle, two other characteristics were also investigated for different chamber conditions. The first one was spray width that was measured at the widest point perpendicular to the spray axis and the second was spray area that was calculated by the colored pixels chosen with predetermined threshold level.

Fuel mass measurements were carried out at 50, 80, 100, 120 MPa injection pressures with 2.0 ms injection duration. In the study of Payri et al. [2], 2000 μs injection duration was used as a quasisteady condition in nozzle characterization. Since the mass absence during needle lift period and additive

Table 3: Experimental conditions.

	Spray tip penetration and cone angle measurements				Autoignition experiments		
Nozzle type	A, B, C, D	A, B, C, D	B	B	A, B, C, D	B	B
Fuel type	ADF	ADF	NH	NH	ADF	NH	CN65
Inj.dur. [ms]	0.4, 0.5, 0.6	1.5	0.4, 0.5, 0.6	1.5	1.5	1.5	1.5
Inj. p [MPa]	80, 100, 120	50	80, 100, 120	50	50	50	50
Ambient p. [MPa]	0.1, 0.6, 2, 3	0.1, 0.6, 2, 3	3	3	3.5	3.5	3.5
Ambient temp. [K]	298	298	298	298	825, 850	825, 850	825, 850

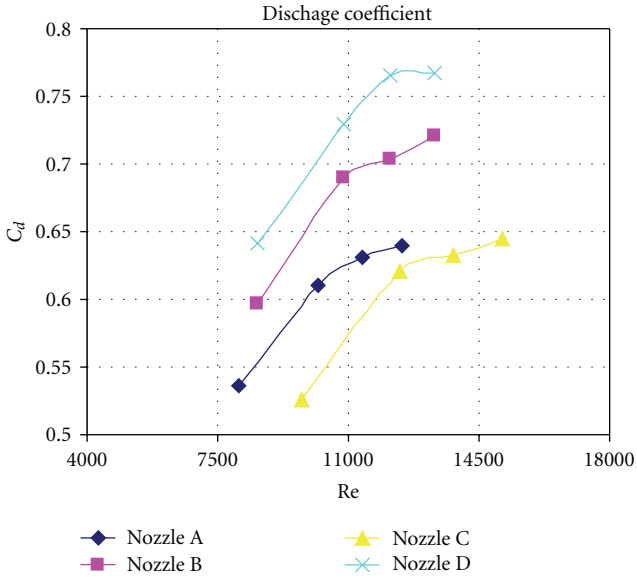

Figure 7: The discharge coefficient change.

mass during closing period may be accepted as equal and needle traveling duration is relatively small compared to 2.0 ms, this rough assumption is acceptable. The injected fuel quantity may vary proportional to the fuel temperature. Thus, the fuel mass measurements were carried out at 75 ± 5°C fuel temperature in order to reduce the weighing errors. To obtain a good estimation of the weighing errors, 400 repetitive injections were gathered in a measurement bottle and weighed with a high precision weighing machine. This procedure repeated at least 4 times in order to get mean mass values of injected fuel.

Discharge coefficient was calculated from (1) and its variation with Reynolds number is depicted in Figure 7. For Nozzle A and C, discharge coefficient has lower values than the others. Since all the injection pressures are in cavitating regions, after a definite gradient change in discharge coefficient curve, it can be concluded that the flow goes into partial hydraulic flip region and supercavitation starts. Making an analogy between the Chaves et al. study [49] and calculated discharge coefficient graphics, the onset of this gradient change is accepted as beginning of supercavitation flow regime. As expected, discharge coefficient is higher and onset of supercavitation starts at higher Re numbers for Nozzle D. It is also expected Nozzle B to follow different path from the C due to inlet rounding by hydrogrinding. Though the discharge coefficient is higher for Nozzle B, the supercavitation starts at, the same injection pressures, but lower Re values with respect to Nozzle C. This result supports the idea that the inlet rounding reduces the flow separation. However, onset of supercavitation didn't change for divergent nozzle, Nozzle A. The discharge coefficient curve of Nozzle A and C are identical. It can be said that the increasing effect of rounding on discharge coefficient is eliminated by nozzle divergent geometry.

For further analyses more measurements are needed, but as a summary, it can be said that the convergent nozzles with hydro-grinding retard the onset of supercavitation and hydrogrinding increases the discharge coefficient. The measured flow experiments showed that the onset of cavitation starts after 10200, 10900, 12300, and 12100 Re number values, which correspond 80, 80, 80 and 100 MPa injection pressures for Nozzle A, B, C, and D, respectively.

4. Experimental Results

4.1. Spray Tip Penetration Measurements. The injected fuel velocity began to increase from zero speed to higher degrees as the needle lifts up. In order to make a comparison between the first four images of different nozzle types, they are given in Figure 8. Since the air in front of the nozzle is quiescent before the injection, velocities of the first droplets get decelerated by the air drag. At this stage, it can be said that the observed spray liquid penetration is relatively short due to low velocities of injected fuel. As the first fuel droplets penetrate into the quiescent air, they push the air in front of the nozzle hole, thus, the initial spray tip penetration is retarded and fuel spray gets wider in radial direction. This is also the reason of the higher spray angles observed at the start of injection which will be presented in the following section. Afterwards, the small flow area restricted by the needle gets wider as it lifts up and the fast penetration period begins. When the needle lifts enough, the fuel flow rate increases and droplets get enough energy to push the ambient air. As a result of this, they penetrate longer. The differences between the upper and lower penetration lengths are visible in Figure 8. It can be said that the nozzle geometry has negligible effect at the initial stages of fuel injection. To reveal ambient pressure and injection pressure effect, the spray tip penetrations under different conditions are presented in Figure 9. The spray tip penetration gets shorter as the ambient pressure gets higher.

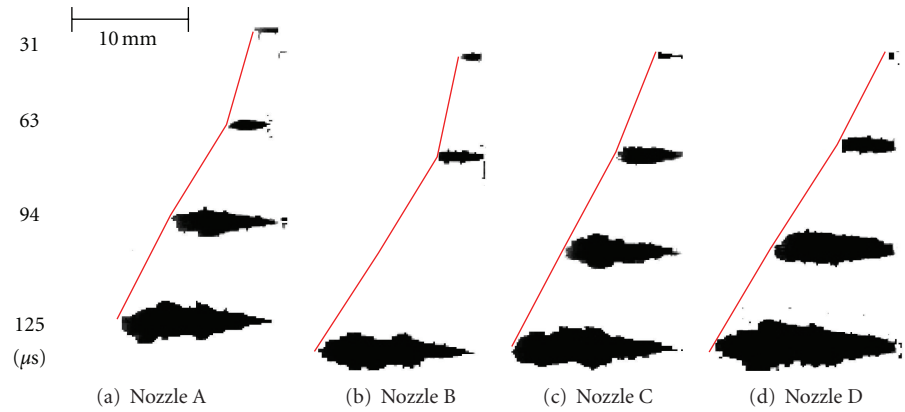

Figure 8: Initial stages of spray evolution for different nozzle types (experimental conditions: 1.5 ms injection duration, 50 MPa injection pressure, 3 MPa ambient pressure, and 300 K ambient temperature).

As expected and concluded by many researchers, higher ambient pressure (or higher ambient density) retards the spray tip penetration. The difference is shorter at the initial stages of spray tip penetrations. The velocity of the upstream region (close to the nozzle) of the spray is much higher than the velocity of downstream region. When the spray lost its velocity at the downstream region, the ambient pressure became effective on the tip penetration results. Besides that it can be said that, at lower ambient pressures, images of the spray tips are foggy, which indicates regions of lower fuel mixture density and the downstream part of the spray has an unclear shape. The spray tip contour gets more visible and the downstream part has elliptical shape at higher pressures.

The injection pressure has significant effect on spray liquid penetration. The effect of increasing pressure on spray tip penetration is depicted in Figure 9(b). The spray tip penetration gets longer as the injection pressure increases. This result is related to both higher quantity and higher velocity of the droplets at higher injection pressures. When the spray lost its momentum related to lower quantity or lower injection pressure, the difference of the penetration lengths got longer at the downstream region of the spray. Proportional to injection pressure, the spray penetrates faster at higher injection pressures.

The injection duration effect and nozzle type effect on spray tip penetration are presented in Figure 10. The injection duration seems to have little effect on spray penetration. Even though all the conditions are equal in Figure 10(a), the penetration length is shorter at 0.4 ms injection duration than the others. This effect may be attributed to the lower injection quantity at 0.4 ms injection duration.

The nozzle type effect on penetration is shown in Figure 10(b). The lower injection penetration of Nozzle A is a result of both lower fuel quantity and its divergent shape At the initial stages, where the injected fuel quantities are close to each other, all nozzles follow similar behavior except the convergent one, Nozzle D. The convergent and hyro-grinded shape of Nozzle D have the potential of suppression of flow separation and cavitation. Due to convergent shape, it has longer penetration length, but after sufficiently long time (after 0.4 ms), as fuel lost its velocity in the ambient air, the penetration length of Nozzle D gets similar to the other nozzles (B and C). Nozzle B and C have the same penetration lengths, which indicates that the bigger nozzle diameter of Nozzles C (sharper inlet) has the same effective nozzle discharge area with Nozzle B (rounded inlet). Effective discharge area reduction increases velocity. As a result, sprays penetration length gets similar with Nozzle B that has lower diameter and rounded inlet.

The predicted spray tip penetrations, by using the equations of Hiroyasu and Arai [21] (3)-(4) and experimental results of Nozzle D are given in Figure 11. The experimental results are very close to predicted ones. However, there are some little discrepancies at the initial stages. Similar discrepancies also have been reported by Kostas et al. [9], and they proposed (9) for initial stages

$$S(t) = At^{3/2}. \tag{9}$$

The derivative of (3) which gives the constant initial tip velocity is not true for real conditions. Kostas et al. [9] obtained the A values from experimental results but no connection was settled between the A and experimental conditions. Similar to Hiroryasu and Arai model, an empirical relation is searched for different injection pressures and ambient conditions for this initial region and it is found that (10) better represents the experimental results. The new breakup time obtained from this equation is very close to previous one

$$S(t) = \left(\frac{\rho_f}{\rho_a}\right)^{0.25} \left(\frac{\rho_a^{1/3}\Delta P}{12\rho_f}\right)^{0.5} t^{3/2} \quad \text{for } 0 < t < t_{\text{break}}. \tag{10}$$

The "A" values of Kostas et al. [9] for some experimental conditions and new modified model results obtained from (10) are listed in Table 4 for comparison.

For the lateral region of the spray evolution, it is found that conicity has disruptive effect on penetration in our experiments as shown in Figure 10(b). It is interesting to observe this disruptive effect on both divergent and

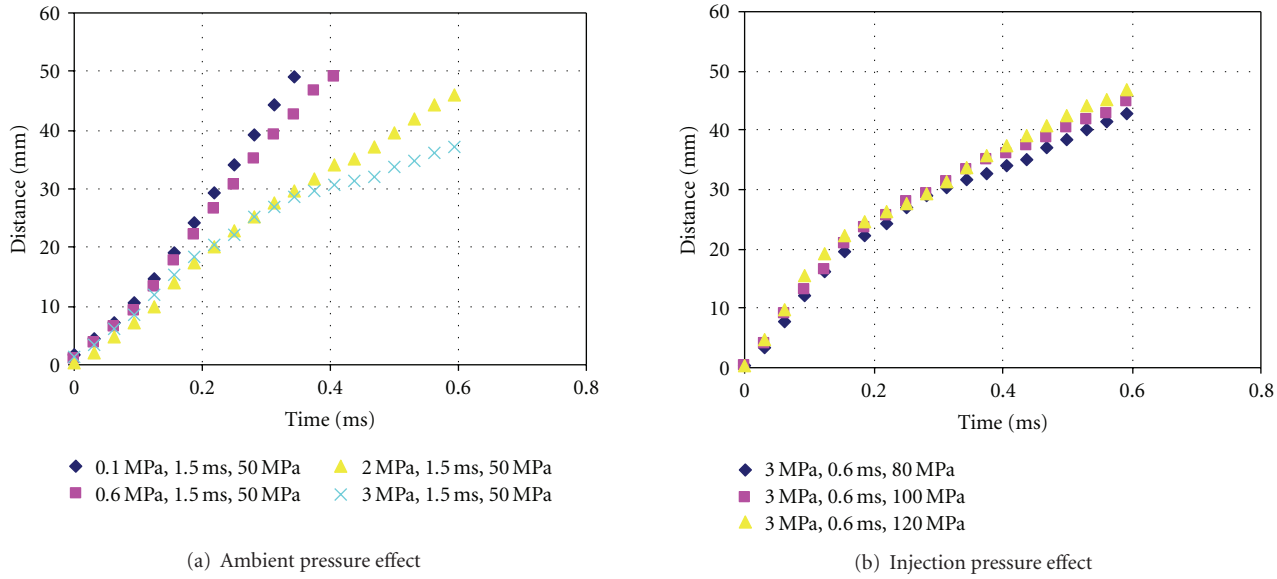

(a) Ambient pressure effect

(b) Injection pressure effect

Figure 9: Spray tip penetrations at 300 K ambient temperature, experimental results with Nozzle D. (a) Ambient pressure effect 1.5 ms injection duration, 50 MPa injection pressure; (b) injection pressure effect 3 Mpa ambient pressure, 0.6 ms injection duration.

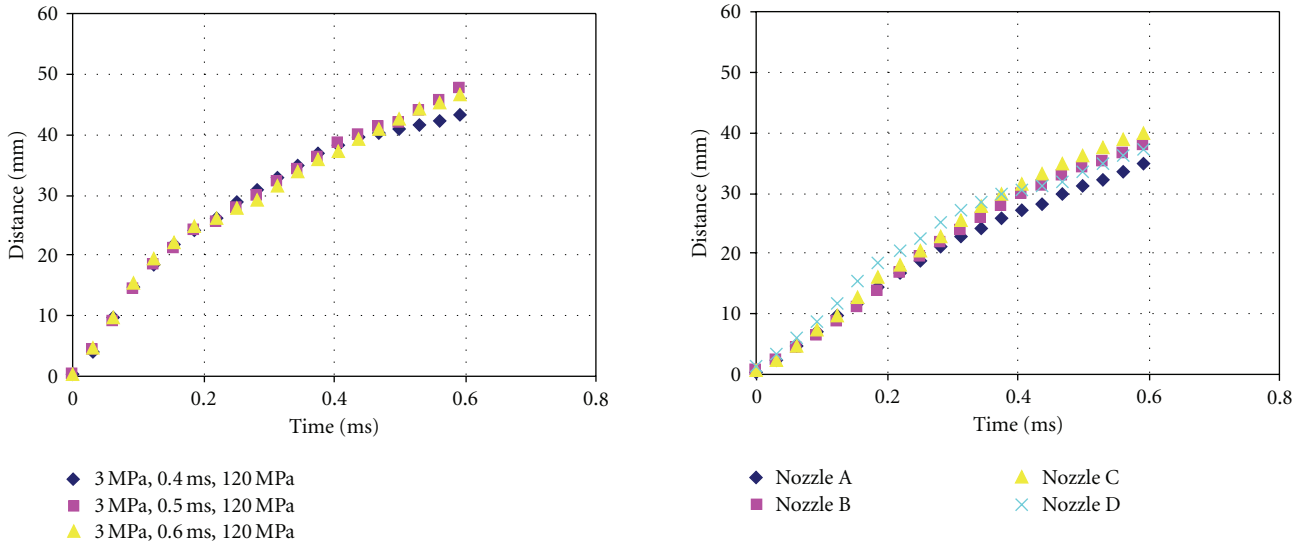

(a) Injection duration effect

(b) Nozzle type effect

Figure 10: Spray tip penetrations at 300 K ambient temperature (a) Injection duration effect, experimental results with Nozzle D, 3 Mpa ambient pressure, 120 MPa injection pressure; (b) nozzle type effect; 3 Mpa ambient pressure, 1.5 ms injection duration, 120 MPa injection pressure.

Table 4: Experimental determined values of "A" from [9] and values of (10).

	"A" values from Kostas et al. [9]		Values obtained from (10)	
	P_{inj} = 50 MPa	P_{inj} = 100 MPa	P_{inj} = 50 MPa	P_{inj} = 100 MPa
Pa = 0.1 Mpa	265 ± 25	570 ± 15	286	573
Pa = 1 Mpa	220 ± 15	565 ± 15	268	538
Pa = 5 Mpa	185 ± 10	480 ± 20	247	507

convergent nozzles. Bae et al. [50] also concludes this effect with experimental results of different positive k-factor nozzle types. They concluded this effect may related to better atomization with smaller cross-section area near the hole exit leading less momentum of each droplet [50]. This explanation seems reasonable for convergent nozzles. Though the droplet size distribution was not measured in this study, the following additional predictions could be made from the experimental results.

(1) It is probable that flow inside the convergent nozzles is less disturbed and does not suffer as much cavitation compared to divergent one, which accelerates spray velocity at initial stages.

(2) This acceleration and convergent shape effect might be resulted with smaller droplets and better atomization for the lateral stages. Resulted smaller droplets shorten the penetration length of spray evolution.

(3) Divergent nozzles have the potential of disturbing the flow inside the nozzle and smaller droplets might be formed at the nozzle exit. As a result of this disruptive effect, penetration length reduces.

However, in previous penetration model, (3), there is no parameter representing the conicity effect. Thus a modification made by introducing a conicity parameter, C_f, into (11) as

$$S(t) = 2.95\left(\frac{\Delta P}{\rho_a}\right)^{1/4}\sqrt{\left(C_f\right)^{Z} d_0 t} \quad \text{for } t \geq t_{\text{break}},\ C_f = \frac{d_i}{d_o}, \tag{11}$$

where d_i is the inner diameter and d_o is the outer diameter of the nozzle. Z is the power of conicity parameter, equals to (-1) for convergent nozzles, $(+1)$ for divergent nozzles and (0) for straight nozzles. If a straight nozzle is used, C_f reduces from (11). Predictions of the new spray tip penetration equation and experimental results are shown in Figure 12. For the initial and lateral regions, more reasonable and more accurate results are obtained with new penetration modeling equations.

Sampling of other experimental values of Nozzle D and predicted data are given in Figure 13. For the initial region, the tip penetrations are better represented by the 3/2th power of time, $(t^{3/2})$. However, some of the experimental results deviate from the predicted ones. Especially at lower ambient pressures, the spray penetrates faster and the predicted penetration line departs from the points of experimental result around the breakup time. This incompatibility is also valid for the predictions of Hiroyasu and Arai model (3).

Accuracy of new penetration model for initial region could be seen at velocity profile. Derivative of the spray tip penetrations are given in (12)-(13), and the comparison with the experimental results are shown in Figure 14. Assuming a constant velocity is not a good representation for initial spray tip velocity. Instead of this, starting from zero velocity, a rapid increase up to the maximum velocity, which is equal to breakup velocity, $U_{S(\max)} = U_{S(\text{break})}$, is observed in the experiments. This maximum velocity is very close to Hiroyasu and Arai constant velocity profile and also it can be said that the new breakup time coincide with the previous one. As it is expected, experiments at higher injection pressure and lower ambient pressure result with higher spray tip velocity:

$$U_s(t) = \frac{3}{2}\left(\frac{\rho_f}{\rho_a}\right)^{0.25}\left(\frac{\rho_a^{1/3}\Delta P}{12\rho_f}\right)^{0.5} t^{0.5} \quad (\text{for } 0 < t < t_{\text{break}}), \tag{12}$$

$$U_s(t) = 2.95\left(\frac{\Delta P}{\rho_g}\right)^{0.25}\left(\frac{\left(C_f\right)^{Z} d}{t}\right)^{0.5} \quad (\text{for } t \geq t_{\text{break}}). \tag{13}$$

The effect of the conicity factor, C_f, reveals itself as lower spray tip velocity for the lateral section of spray evolution. Though the difference is very little, the effect of C_f could give information for parametric investigation. The effect of the conicity could be better seen with a nozzle, which has exaggerated conicity. This suggestion may be considered in future works. Before concluding on spray penetration experiments it must be emphasized that more and advanced experiments are needed for close nozzle region investigations.

Spray macroscopic characteristic at evaporating conditions has widespread research area. It is known that, ambient temperature has reducing effect on spray liquid penetration. Since the droplets evaporate faster at higher temperatures, they lost their momentum to penetrate faster. Evaporation of the droplets make the spray jet invisible and it gets less detectable as the temperature increase. Temperature effect on spray liquid penetration and spray projection area are presented in Figure 15.

When the first droplets get into the high temperature environment, they evaporate very fast and the liquid penetration length reduces relatively. As the time progresses the new droplets get into the chamber and as they evaporate, they also reduce the temperature locally. Thus, the evaporation rate reduces and they beginto penetrate higher lengths. After some certain time (approximately after 0.3 ms), the increase seen at the spray liquid penetration plot could be explained by this evaporation rate-related velocity increase. As the spray jet move forward, the downstream part of the spray gets wider and much more hot air from the surrounding gas meets with warmer droplets. As a result of this process, the liquid spray jet reaches a steady penetration length and it cannot go further. The spray momentum wafts evaporated spray and fuel spray might go further with very small diameter droplets which are about to vanish. The steady liquid penetration length reduces, as the temperature gets higher. The above explanation is also valid for the variation of the spray projection area. At the initial stages, the spray projection area grows slowly, then it accelerates and reaches a constant degree after a certain time.

4.2. Cone Angle Measurements. The measurements of the spray cone angle generally follows a decreasing path at the initial regions and reaches a constant value after the spray develops, as most of the results presented in the literature. In

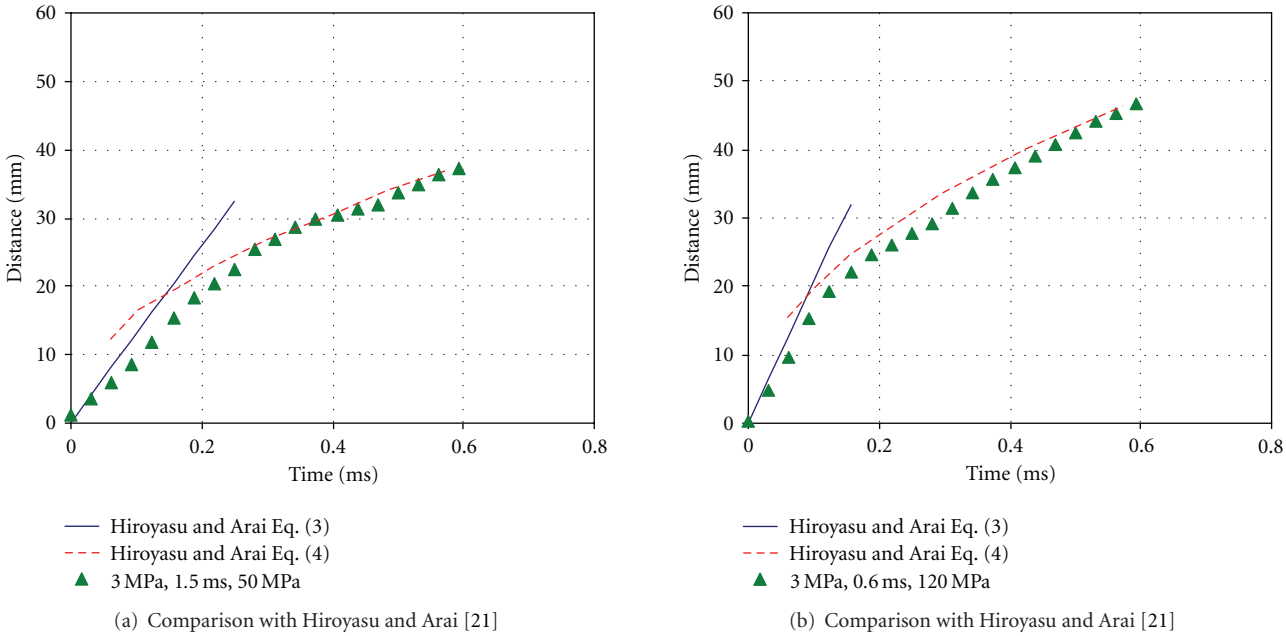

(a) Comparison with Hiroyasu and Arai [21]

(b) Comparison with Hiroyasu and Arai [21]

Figure 11: Experimental results of spray tip penetration and Hiroyasu and Arai model prediction, Nozzle D.

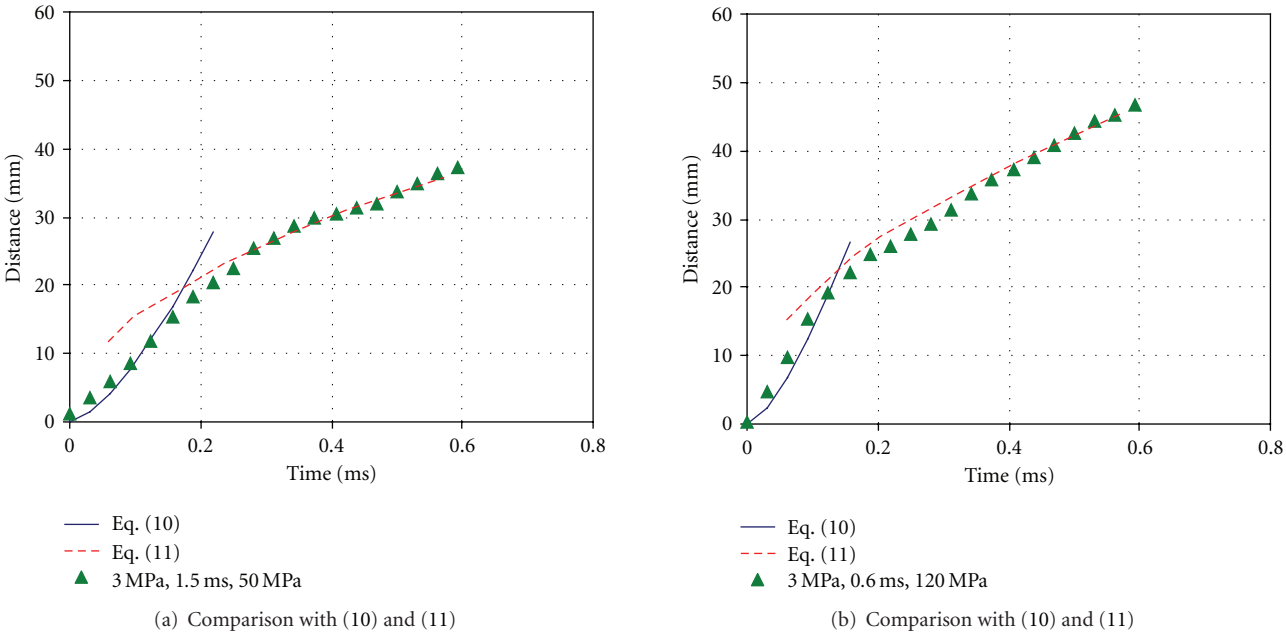

(a) Comparison with (10) and (11)

(b) Comparison with (10) and (11)

Figure 12: Comparison of experimental results with (10) and (11), Nozzle D.

this part, cone angle, spray width and spray projection area measurements will be presented together in order to make a judgment about the spray evolution.

All the cone angle results are very close to each other which cause to make a certain distinguish impossible. Nevertheless, the differences are relatively higher at lower ambient pressures. Cone angle measurements for different nozzle types, showing ambient pressure effect, are presented in Figure 16. The spray width growths of the same experiments could be seen on Figure 17. At lower ambient pressures, Nozzle A has wider cone angle due to its divergent shape, Nozzle B and C follows the same path with each other and Nozzle D has narrowest cone angle which may be attributed to its convergent shape. The discrepancies between the cone

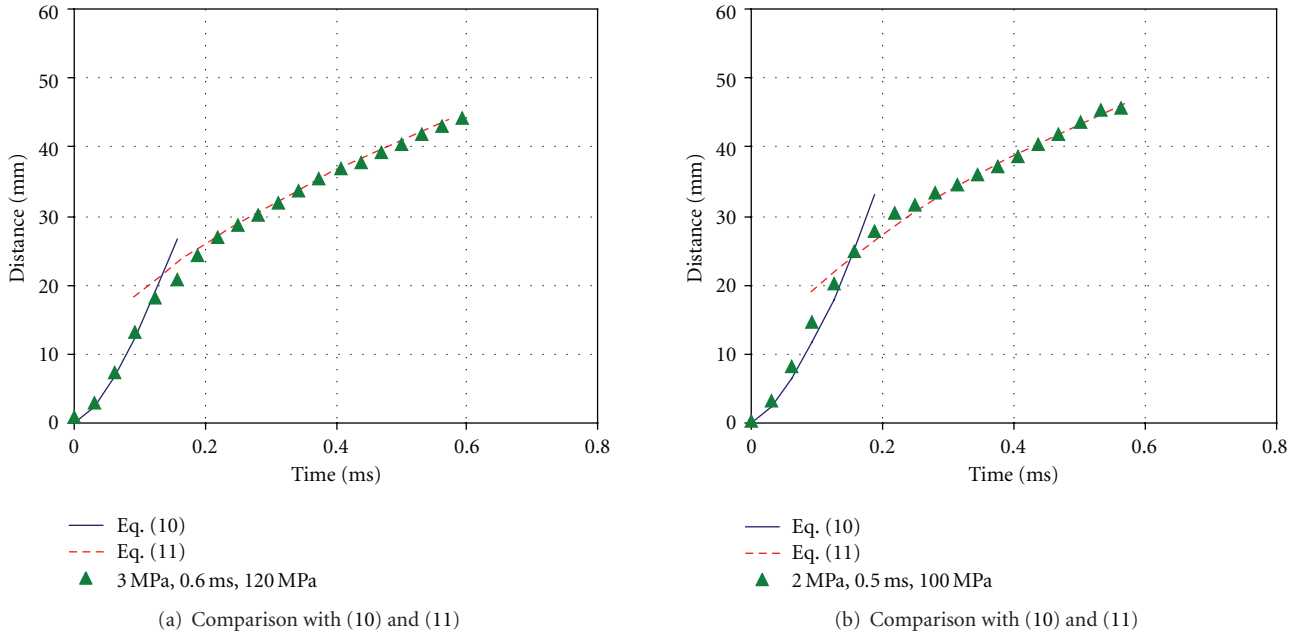

Figure 13: Comparison of experimental results with (10) and (11), Nozzle A.

angle measurements get lost at higher ambient pressures. They have more or less the same cone angle for the period after 0.5 ms.

Spray width growths depicts a different picture than cone angle results. At low ambient pressures, Nozzle A and D has the same spray widths. And after 0.4 ms, the Nozzle D has the widest spray profile. This result is related to the penetration length of Nozzle D. Though Nozzle D has lower cone angle at lower ambient pressures, it penetrates faster and the spray width gets wider than other type of nozzles' widths. The spray widths of the Nozzle B and C coincide with each other. At higher pressures, all spray widths are approximately the same level. However, Nozzle D has the widest spray width after 0.4 ms because of the longer spray penetration.

In general, it can be said that spray cone angle is very similar to each other at elevated pressures. This is why, it is an unavailing attempt to search for nozzle type effect on cone angle. Thus, cone angle analyses confined with the comparison of Hiroyasu and Arai model, (5). The predicted cone angle measurements with experimental results of Nozzle B and spray projection area growth are plotted in Figure 18. For the lateral stages of spray development, the predicted results are in consistence with the experimental results. It can be said that, the ambient pressure has increasing effect on cone angle and a decreasing effect on spray projection area. The appreciable effect is shown after the spray developed enough. Though ambient pressure has decreasing effect on spray projection area at the initial stages, this effect vanishes and reverses as the spray propagates long enough. It can be concluded from the projection area measurements that; at lower ambient pressures the spray spreads to a wider area resulting lower fuel concentration than higher ambient pressures.

4.3. Autoignition Measurements. At higher injection pressures the spray quickly cross the optically monitored region and if high amount of fuel injected, spray wall impingement is inevitable on bottom cover of the vessel. In order to avoid this condition, the main ignition experiments were done at 50 MPa injection pressure. Three sequences of ignition, autoignition, developed ignition and fading are depicted with tree images in Figure 19. The autoignition is detected by the illumination intensity change of the recorded images.

The first three pictures consists chemiluminescence and autoignition of premixed air-fuel mixture. A rapid increase in flame luminosity is observed at this period. Approximately 0.1 ms after the first luminosity detected, all the spray downstream part covered with flame. Then, at fully developed combustion period, the diffusion combustion starts and the ignition gets closer to the nozzle tip when spray loses the repelling effect of injection. This period is observed after the end of fuel injection. Later, fuel combustion continues at the downstream part of the spray pattern where fuel droplets evaporate and meet with fresh air. At this period, turbulent combustion continues but it fades away through to the bottom section of the chamber.

The autoignition experiments have showed that the nozzle type effect has little influence on autoignition delay and autoignition zone. Four different nozzle types and their ignition delay time versus temperature plots are given in Figure 20. There is also a predicted ignition delay plots of Pischinger's equation, (7), and Fujimoto's equation, (8), in the graphic. It is seen that Pischinger's equation is over predict the ignition delay time. This deviation is related to the experimental setup and tested fuels. In the study of Pischinger, they used a continuous air flow in the combustion chamber.

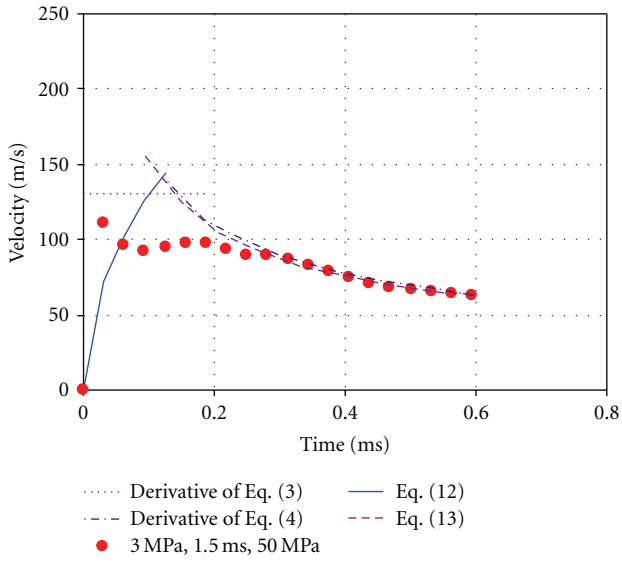

(a) Comparison of old and new models $P_{inj} = 50$ MPa, $P_{amb} = 3$ MPa

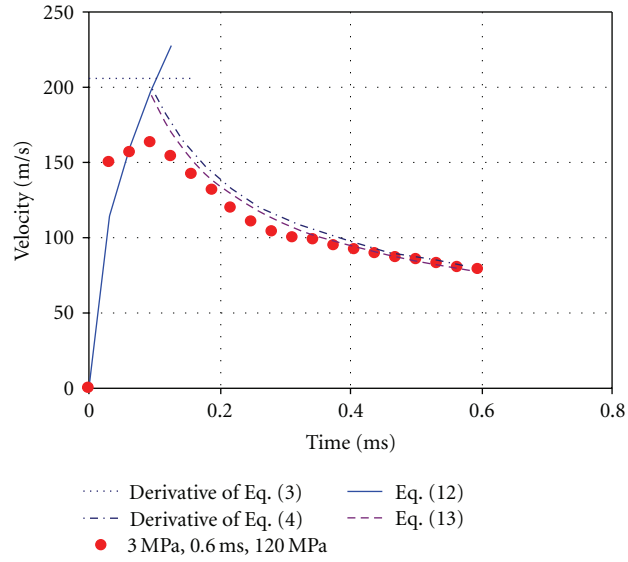

(b) Comparison of old and new models $P_{inj} = 120$ MPa, $P_{amb} = 3$ MPa

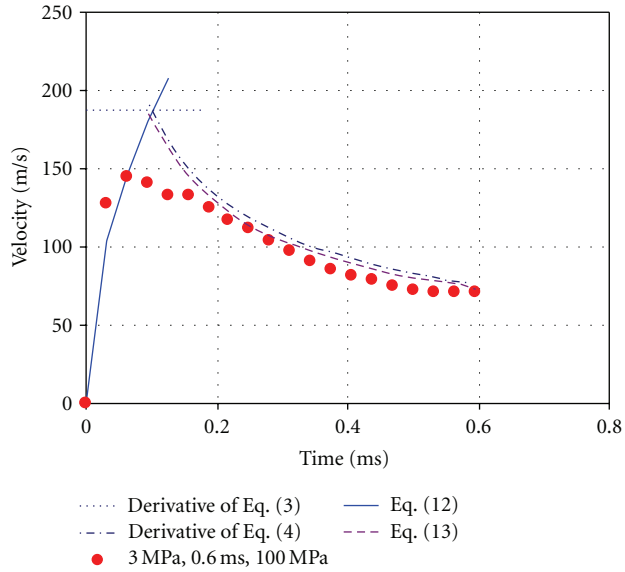

(c) Comparison of old and new models $P_{inj} = 100$ MPa, $P_{amb} = 3$ MPa

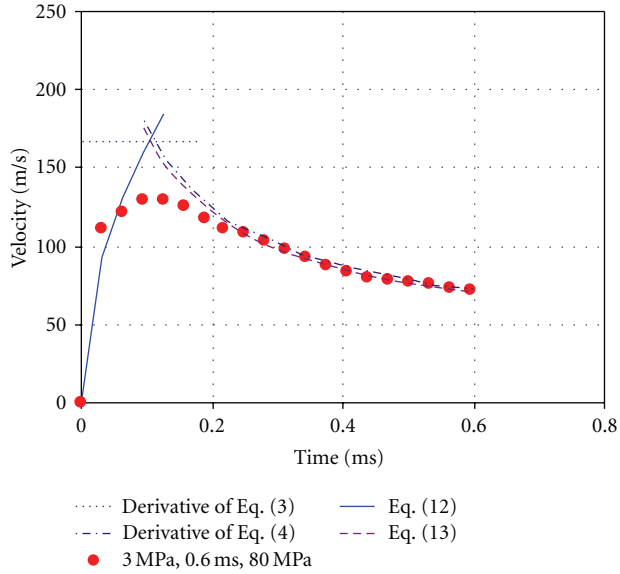

(d) Comparison of old and new models $P_{inj} = 80$ MPa, $P_{amb} = 3$ MPa

Figure 14: Spray velocity profiles, old and new models, Nozzle D.

It can be seen that the experimental results agree with the Fujimoto's equation. There is also some dissimilarity between the experiments carried under same conditions. This might be caused from the nature of diesel ignition experimental study. The small discrepancies might also be related to the radiation effect of heater element used in the experiments, which is not measured.

From the plots of Figure 20, it is seen that tested nozzles, which have different inlet geometries but similar macroscopic properties, have very similar ignition behaviour. When ambient temperature is below 800°K, all nozzles suffers relatively long ignition delay period, approximately 1.8 ms. Higher ambient temperatures reduces the ignition delay time to around 1.0 ms. The location of autoignition is also independent from nozzle type. A common result for all type of nozzles come in view as ignition location gets closer to the nozzle at higher ambient temperatures.

Autoignition experiments show that little nozzle differences on inlet geometry make no visible change on ignition delay time and autoignition location.

The first two images, on which illumination increase is observed, are presented in Figure 21 to show ignition similarity of different nozzle types. It can be concluded that liquid spray evaporates very fast and adequate mixture of fuel-air is obtained in all tested nozzles at the same time periods. Though, it is probable that different nozzle geometries might

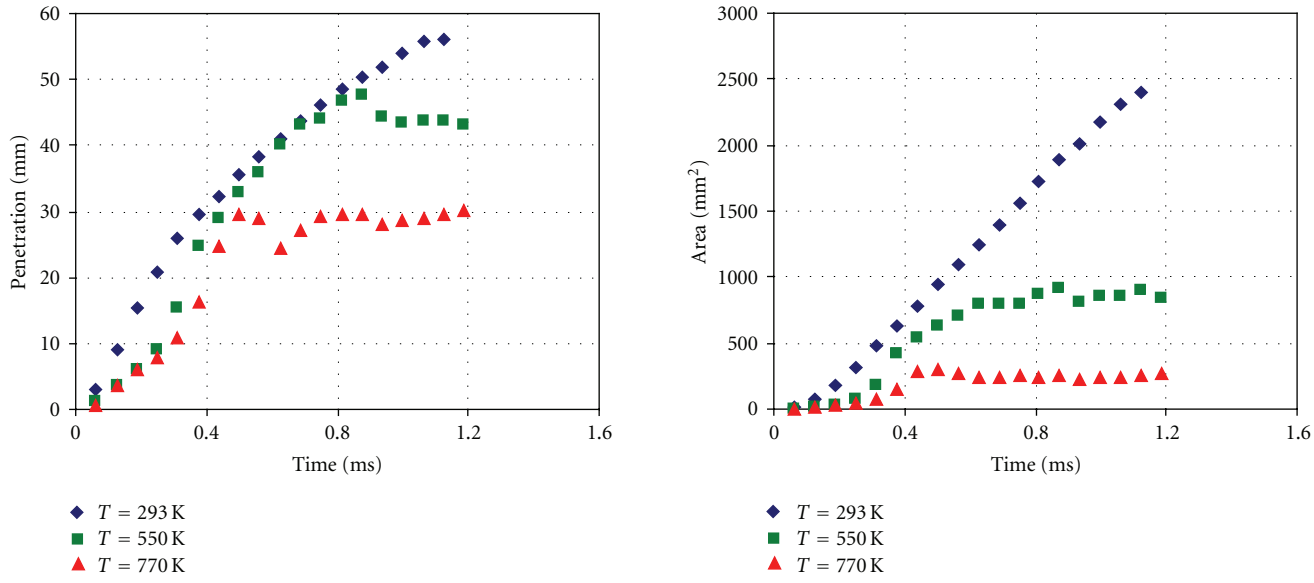

(a) Ambient temperature effect

(b) Spray projection area

Figure 15: Ambient temperature effect on (a) spray liquid penetration and (b) spray projection area (experimental results obtained with Nozzle B, at 3 MPa ambient pressure, 50 MPa injection pressure, 1.5 ms injection duration).

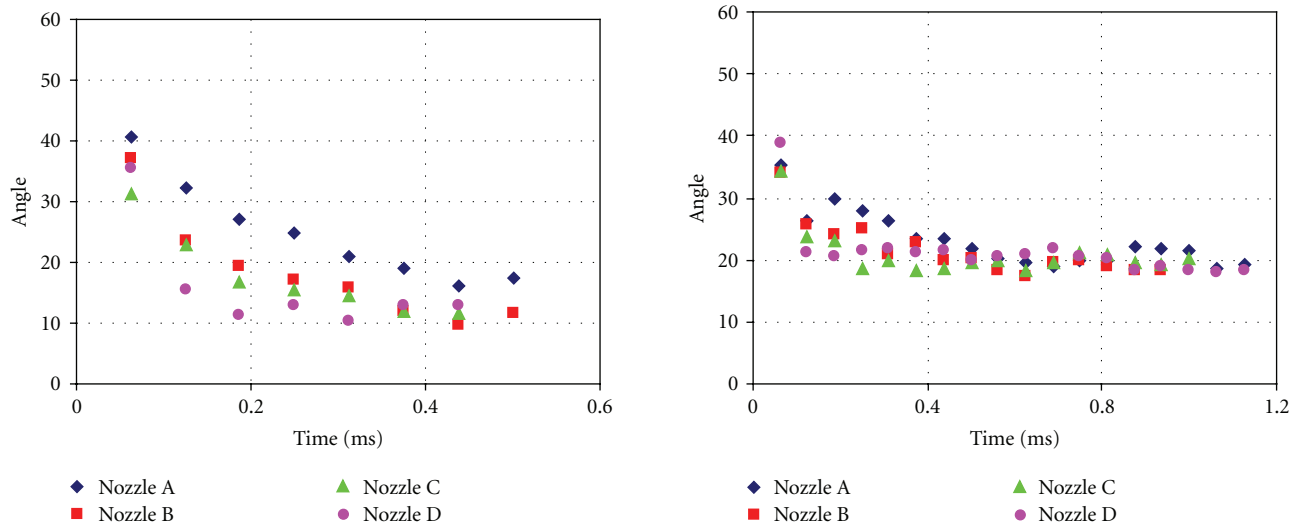

(a) Spray angle measurements at 0.1 MPa ambient pressure

(b) Spray angle measurements at 3 Mpa ambient aressure

Figure 16: Comparison of spray angle measurement in terms of nozzle type (300 K ambient temperature, 50 MPa injection pressure, 1.5 ms injection duration).

results with different microscopic properties, autoignition characteristics are very similar for tested ones.

At lower ambient temperatures, ignition delay gets longer and autoignition takes place at downstream part of the chamber. When the temperatures gets higher, ignition delay time gets lower and also autoignition takes place still at downstream part of the spray but closer to the nozzle tip. It is seen that convergent nozzle, (Nozzle D), has smaller ignition delay time and autoignition occurs at relatively farther place, but the differences are very small.

Self ignition is highly effected from ambient temperature. To reveal the cetane number effect, the ignition characteristic of different fuel types are investigated with Nozzle B at 773–828 K ambient temperature range and the results were plotted in Figure 22. CN65 fuel has approximately 10% shorter ignition delay periods than the other tested fuels.

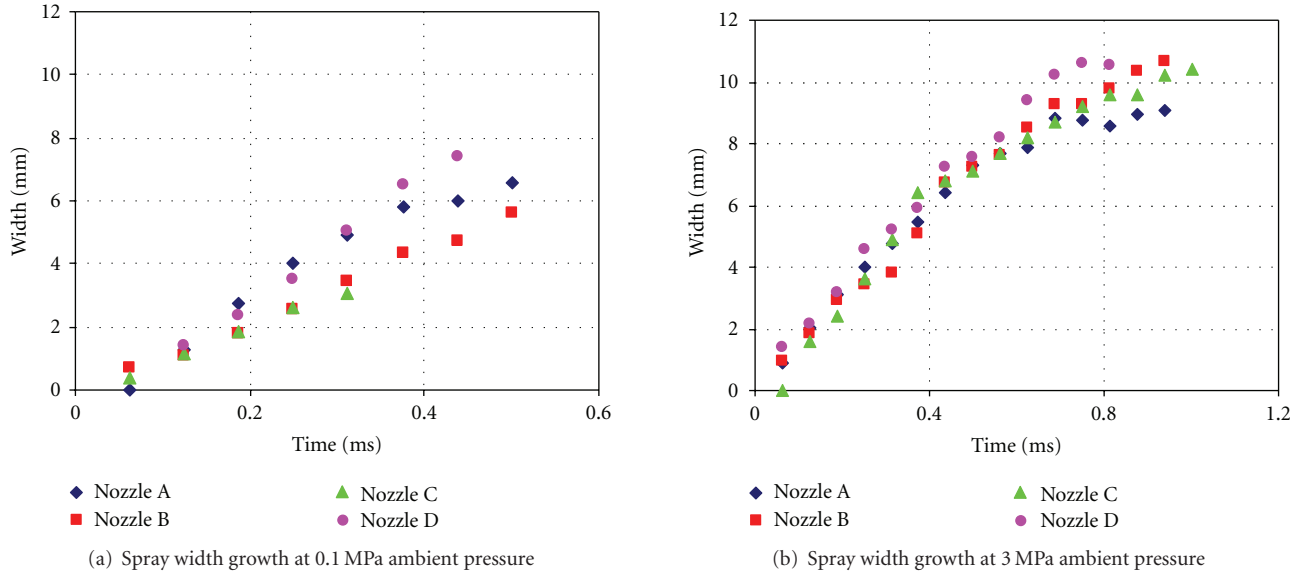

(a) Spray width growth at 0.1 MPa ambient pressure

(b) Spray width growth at 3 MPa ambient pressure

Figure 17: Comparison of spray width growth in terms of nozzle type (50 MPa injection pressure, 1.5 ms injection duration).

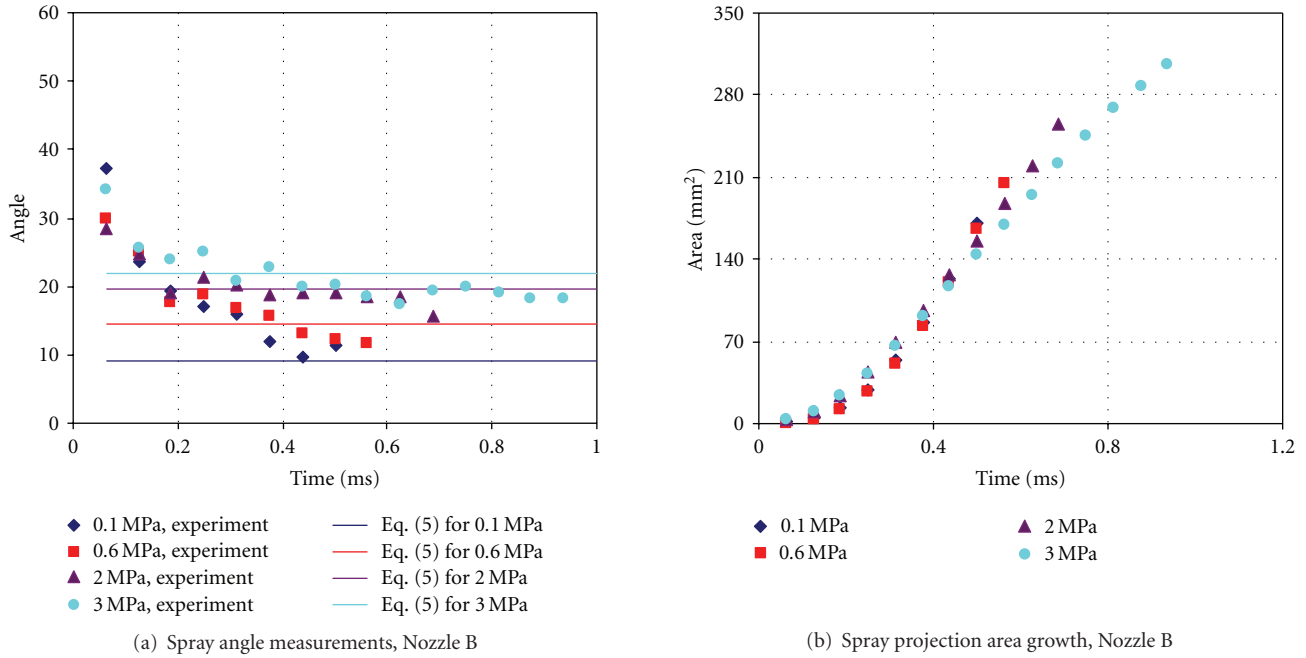

(a) Spray angle measurements, Nozzle B

(b) Spray projection area growth, Nozzle B

Figure 18: Effect of ambient pressure, Nozzle B measurements, (a) variation of spray angle by ambient pressure, (b) Variation of pressure spray projection area by ambient pressure (50 MPa injection pressure, 1.5 ms injection duration).

It must be stated that there are small shot-to-shot variations in ignition delay time and self-ignition regions. Especially, there is no rule for self-ignition location depending on fuel type. It can be noted that, since it has lower ignition delay periods, CN65 fuel type has closer self-ignition regions (except for a few experiments apart from general tendency). However, the ignition location results do not reveal a clear and distinguishable reduction. The other tested fuels have also similar ignition locations.

Since it is one component, in numerical simulations *n*-heptane is generally chosen to represent diesel fuel. In the constant volume experiments of this study, *n*-heptane is also tested to observe its ignition delay properties. Ignition delay and ignition characteristics of *n*-heptane are very similar to the ones that of diesel fuel. After autoignition, it is observed that the flame of *n*-heptane spreads faster than the other tested fuels, which is a result of its higher volatility. This fuel is specially tested to use its data in future numerical

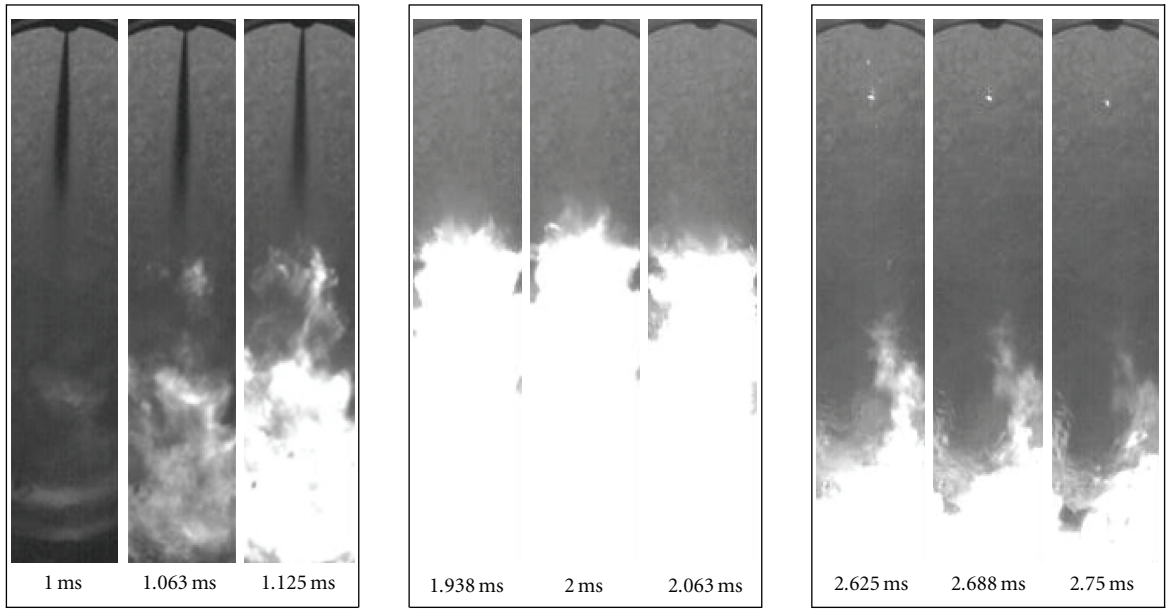

(a) Autoignition (b) Developed ignition (c) Ignition fading

Figure 19: Image sets taken from different ignition sequences of the diesel fuel with Nozzle C (3.5 MPa ambient pressure, 828 K ambient temperature, 50 MPa injection pressure, 1.5 ms injection duration).

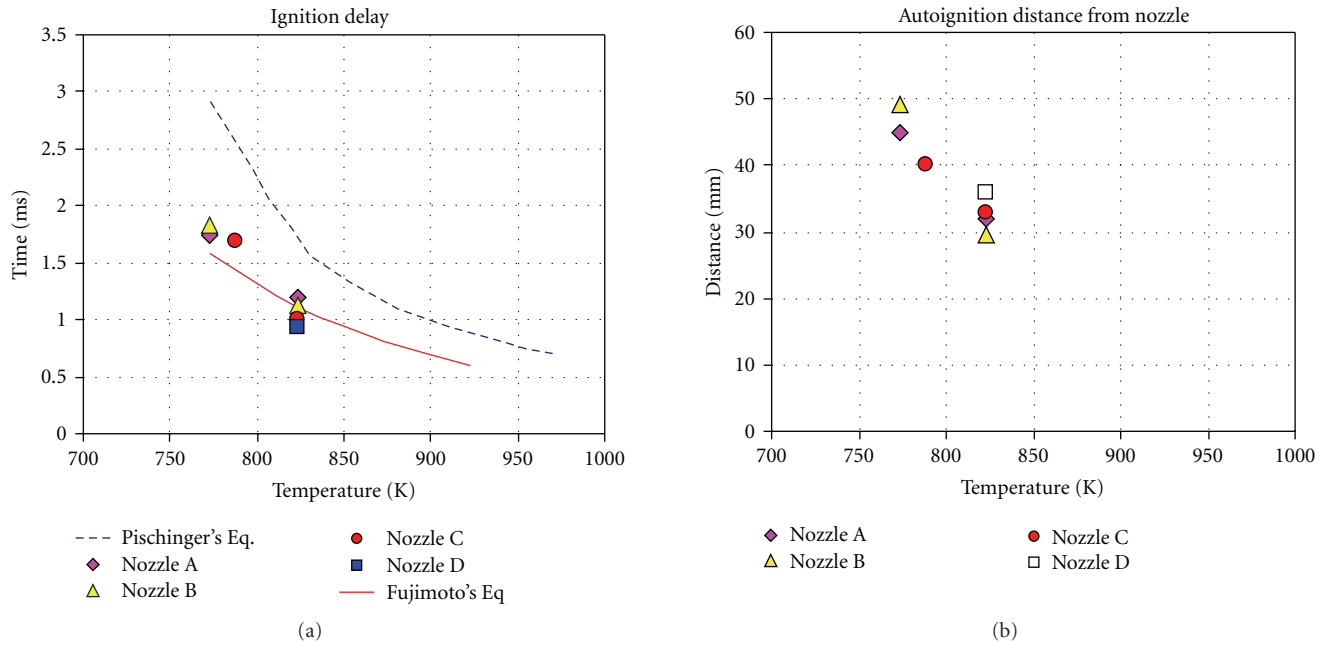

(a) (b)

Figure 20: Ignition delay time and autoignition distance from nozzle tip for different type of nozzles (3.5 MPa ambient pressure, 50 MPa injection pressure, 1.5 ms injection duration).

works. As a conclusion, it can be said that *n*-heptane is a good representative of diesel fuel for its self-ignition properties.

Ignition experiments showed that autoignition starts at the downstream regions of the spray similar to the Dec's conceptual model [41]. Recent advances in injection systems bring higher injection pressures. As a result of this, fuel injected with higher injection velocities. Thus, spray carries the fuel-vapor and combustible air-fuel mixture through to the downstream regions where remainder fuel rapidly vaporizes with the entrained hot-air. Observed ignition locations are all at the downstream section of the spray and generally ignition starts at multiple points.

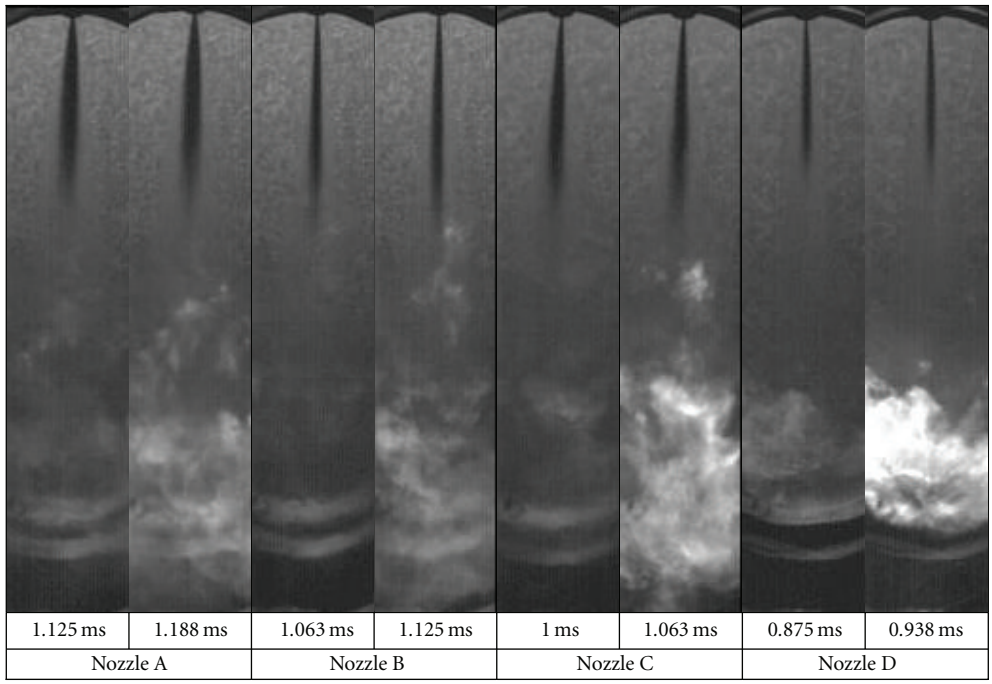

Figure 21: The autoignition images of different nozzle types.

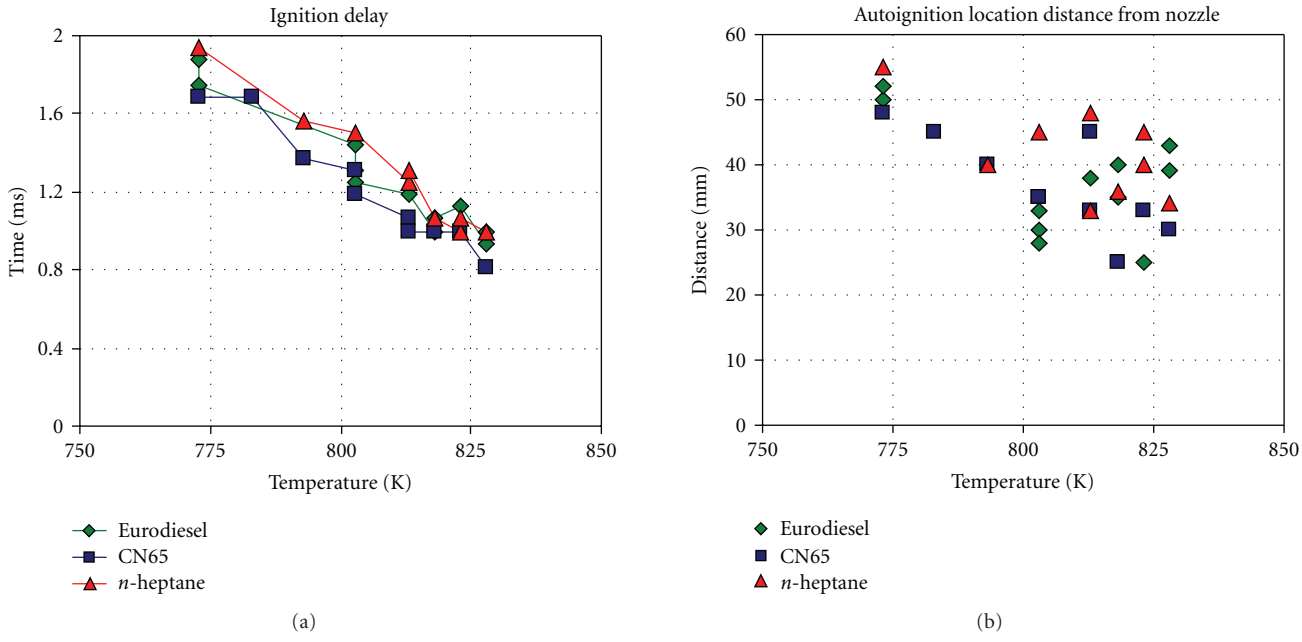

Figure 22: Ignition delay time and autoignition location distance from nozzle tip for different type of fuels (3.5 MPa ambient pressure, 50 MPa injection pressure, 1.5 ms injection duration).

5. Conclusions

In order to study macroscopic spray characteristics and autoignition properties of different type of nozzles, a constant volume combustion chamber was manufactured and diesel engine conditions were obtained in the experimental setup. Four different kind of nozzle and three different kind of fuel were tested in the test facility. A CCD camera was used to obtain spray images and a digital imaging program was used to obtain corrected images. Digitalization allows

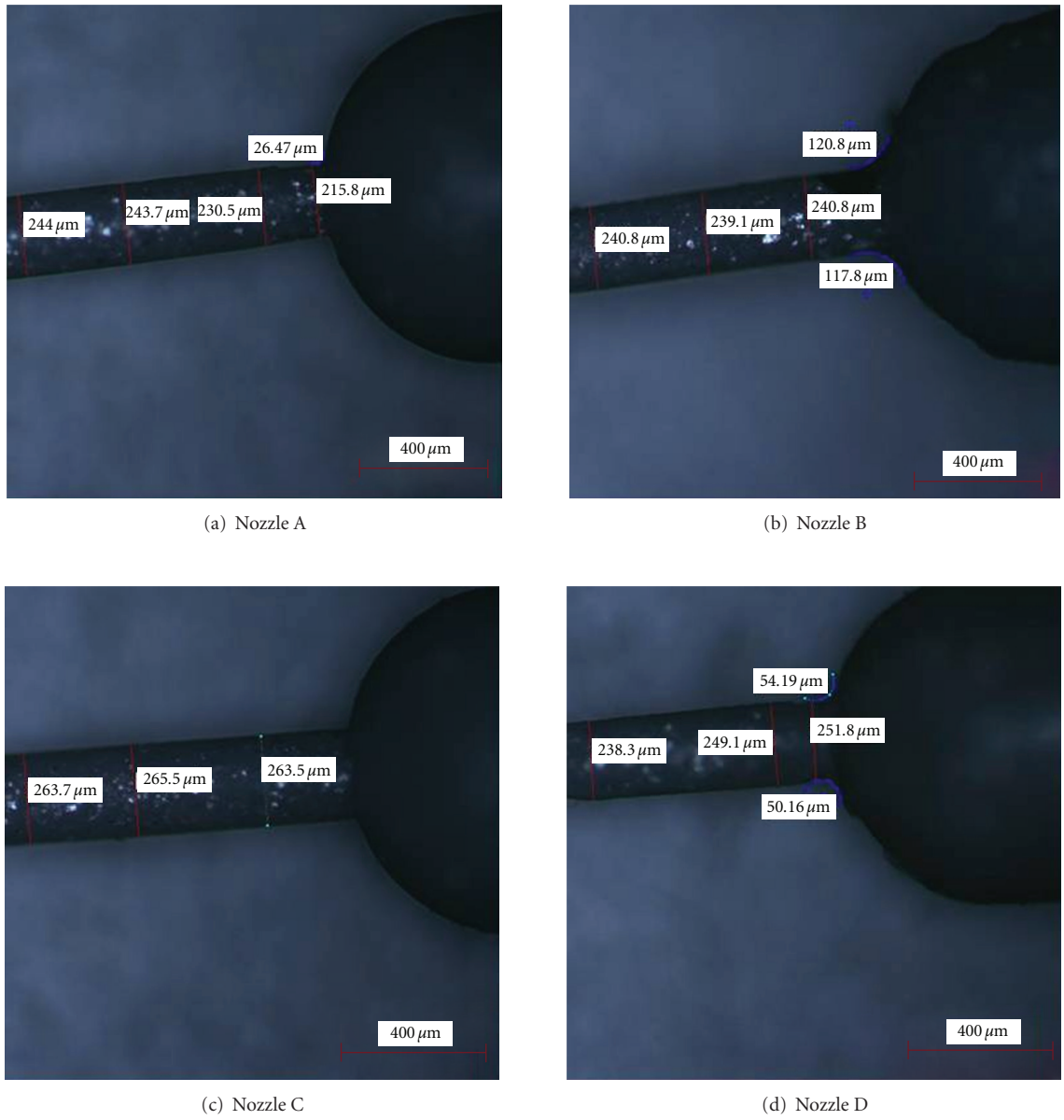

(a) Nozzle A

(b) Nozzle B

(c) Nozzle C

(d) Nozzle D

Figure 23: The silicon mold measurements of nozzle holes.

objectively determining spray characteristics. Experimental results were compared with well-known spray correlations published in the literature. From the analyses of the experimental study, the following conclusions are revealed.

(1) Conicity and hydrogrinding increase discharge coefficients. Convergent nozzle has higher and divergent nozzle has smaller discharge coefficients. All the nozzles orifices experience supercavitation condition. However, the convergent nozzles may retard the onset of cavitation to the higher injection pressures.

(2) The spray liquid penetration starts from zero velocity at the nozzle exit and reaches maximum velocity at around breakup time.

(3) Spray liquid penetration decreases as the ambient pressure or temperature increases. Higher injection pressure, lower injection quantities have increasing effect and conical nozzles (divergent and convergent) have decreasing effect on spray liquid penetration.

(4) Spray cone has wider angles at the initial stages of spray evolution. Cone angle decreases as the spray penetrates, and, after the spray developed enough, the spray cone angle settles to constant value.

(5) Spray cone angle increase as the ambient pressure increase. Injection pressure and conicity have inconsiderable effect on developed spray cone angle.

(6) Generally, autoignition observed at unsettled downstream part of the injected fuel spray. The indefinite

location of autoignition gets closer to the injector tip—but still at the downstream section—as the temperature gets higher.

(7) Though there are little differences between the tested nozzle geometries, the ignition delay periods are very close to each other. There is no detectable discrepancy at ignition delay period and self-ignition location.

(8) Cetane number has decreasing effect on ignition delay. However, this effect has small distinctions on ignition delay periods of tested fuels (fuels that have cetane numbers above 55).

(9) *N*-heptane has similar autoignition characteristics with diesel fuel. It can be used as a representative fuel for diesel investigations.

To better represent the spray liquid penetration, the models proposed by Hiroyasu and Arai were enhanced by adding new coefficients representing nozzle conicity. The acceptance of initial steady maximum velocity of previous model is also modified with the new empirical equation for initial stage of spray evolution, which includes injection parameters. The new models for spray liquid penetrations very well describe the experimental results.

Time-dependent variation of spray cone angle is also an interesting physical observation. A correlation could be settled for cone angle dependency that is observed at initial stages. This conclusion may be considered in the future study.

Appendix

See Figure 23.

Nomenclature

C_d: Discharge coefficient
m_f: Actual fuel flow
m_{th}: Theoretical fuel flow
A_0: Area of nozzle outlet
ρ_f: Fuel density
P_{inj}: Injection pressure
P_{back}: Pressure of the injection environment
u_{eff}: Effective spray velocity
A_{eff}: Effective area of nozzle outlet
u_{mean}: Mean spray velocity
ρ_a: Density of the injection environment
S: Spray tip penetration
ΔP: Differential pressure of inlet and exit of nozzle
d_0: Nozzle outlet diameter
l: Nozzle hole length
d_{sack}: Sack chamber diameter of nozzle hole
τ: Ignition delay time.

References

[1] E. Delacourt, B. Desmet, and B. Besson, "Characterisation of very high pressure diesel sprays using digital imaging techniques," *Fuel*, vol. 84, no. 7-8, pp. 859–867, 2005.

[2] R. Payri, F. J. Salvador, J. Gimeno, and L. D. Zapata, "Diesel nozzle geometry influence on spray liquid-phase fuel penetration in evaporative conditions," *Fuel*, vol. 87, no. 7, pp. 1165–1176, 2008.

[3] I. V. Roisman, L. Araneo, and C. Tropea, "Effect of ambient pressure on penetration of a diesel spray," *International Journal of Multiphase Flow*, vol. 33, no. 8, pp. 904–920, 2007.

[4] R. J. H. Klein-Douwel, P. J. M. Frijters, L. M. T. Somers, W. A. de Boer, and R. S. G. Baert, "Macroscopic diesel fuel spray shadowgraphy using high speed digital imaging in a high pressure cell," *Fuel*, vol. 86, no. 12-13, pp. 1994–2007, 2007.

[5] S. S. Sazhin, G. Feng, and M. R. Heikal, "A model for fuel spray penetration," *Fuel*, vol. 80, no. 15, pp. 2171–2180, 2001.

[6] J. M. Desantes, R. Payri, F. J. Salvador, and A. Gil, "Development and validation of a theoretical model for diesel spray penetration," *Fuel*, vol. 85, no. 7-8, pp. 910–917, 2006.

[7] H. K. Suh, S. W. Park, and C. S. Lee, "Effect of piezo-driven injection system on the macroscopic and microscopic atomization characteristics of diesel fuel spray," *Fuel*, vol. 86, no. 17-18, pp. 2833–2845, 2007.

[8] R. Payri, F. J. Salvador, J. Gimeno, and J. de la Morena, "Study of cavitation phenomena based on a technique for visualizing bubbles in a liquid pressurized chamber," *International Journal of Heat and Fluid Flow*, vol. 30, no. 4, pp. 768–777, 2009.

[9] J. Kostas, D. Honnery, and J. Soria, "Time resolved measurements of the initial stages of fuel spray penetration," *Fuel*, vol. 88, no. 11, pp. 2225–2237, 2009.

[10] A. Doudou, "Turbulent flow study of an isothermal diesel spray injected by a common rail system," *Fuel*, vol. 84, no. 2-3, pp. 287–298, 2005.

[11] L. Fu-shui, Z. Lei, S. Bai-gang, LI. Zhi-jie, and H. J. Schock, "Validation and modification of WAVE spray model for diesel combustion simulation," *Fuel*, vol. 87, no. 15-16, pp. 3420–3427, 2008.

[12] J. S. Hwang, J. S. Ha, and S. Y. Na, "Spray characteristics of DME in conditions of common rail injection system(II)," *International Journal of Automotive Technology*, vol. 4, no. 3, pp. 119–124, 2003.

[13] W. Ning, *Development of a next-generation spray and atomization model using an Eulerian-Langrangian methodology*, Ph.D. thesis, University of Wisconsin-Madison, 2007.

[14] C. Crua, *Combustion processes in a diesel engine*, Ph.D. thesis, University of Brighton, 2002.

[15] A. Malave-Sanabria, *Diesel spray imaging using X-rays*, Ph.D. thesis, University of Wisconsin-Madison, 2007.

[16] K. H. Goney, *Investigations of internal Nozzle multiphase flow and its effects on diesel sprays*, Ph.D. thesis, University of Wisconsin-Madison, 1999.

[17] J. Shao and Y. Yan, "Digital imaging based measurement of diesel spray characteristics," *IEEE Transactions on Instrumentation and Measurement*, vol. 57, no. 9, pp. 2067–2073, 2008.

[18] J. Naber and D. L. Siebers, "Effects of gas density and vaporisation on penetration and dispersion of Diesel sprays," SAE Paper, 960034, 1996.

[19] Y. Wakuri, M. Fujii, T. Amitani, and R. Tsuneya, "Studies of the penetration of fuel spray in a diesel engine," *Bulletin of Japan Society of Mechanical Engineers*, vol. 3, no. 9, 1960.

[20] J. C. Dent, "A basis for the comparison of various experimental methods for studying spray penetration," *Transactions of the SAE*, vol. 80, pp. 1881–1884, 1971.

[21] H. Hiroyasu and M. Arai, "Structure of Fuel Sprays in Diesel Engines," SAE Paper, 900475, 1990.

[22] L. C. Ganippa, S. Andersson, J. Chomiak, and A. Matsson, "Combustion characteristics of diesel sprays from equivalent nozzles with sharp and rounded inlet geometries," *Combustion Science and Technology*, vol. 175, no. 6, pp. 1015–1032, 2003.

[23] D. Verhoeven, J. L. Vanhemelryck, and T. Baritaud, "Macroscopic and ignition characteristics of high-pressure sprays of single-component fuels," SAE Paper, 981069, 1998.

[24] J. M. Desantes, R. Payri, J. M. Garcia, and F. J. Salvador, "A contribution to the understanding of isothermal diesel spray dynamics," *Fuel*, vol. 86, no. 7-8, pp. 1093–1101, 2007.

[25] H. K. Suh and C. S. Lee, "Effect of cavitation in nozzle orifice on the diesel fuel atomization characteristics," *International Journal of Heat and Fluid Flow*, vol. 29, no. 4, pp. 1001–1009, 2008.

[26] M. C. Lai, T. C. Wang, X. Xie et al., "Microscopic characterization of diesel sprays at VCO nozzle exit," SAE Technical paper, 982542, 1998.

[27] J. M. Desantes, J. V. Pastor, J. M. Pastor, and J. E. Juliá, "Limitations on the use of the planar laser induced exciplex fluorescence technique in diesel sprays," *Fuel*, vol. 84, no. 18, pp. 2301–2315, 2005.

[28] T. Parker, E. Jepsen, and H. McCann, "Measurements and error analysis of droplet size in optically thick diesel sprays," in *Proceedings of the 27th International Symposium on Combustion*, pp. 1881–1888, The Combustion Institute, 1998.

[29] P. Rantanen, A. Valkonen, and A. Cronhjort, "Measurements of a diesel spray with a normal size nozzle and a large-scale model," *International Journal of Heat and Fluid Flow*, vol. 20, no. 5, pp. 545–551, 1999.

[30] T. Kim, *Quantitative 2-D fuel vapor concentration measurements in an evaporating diesel spray using exciplex fluorescence method*, Ph.D. thesis, University of Wisconsin-Madison, 2001.

[31] T. Boëdec, J. C. Champoussin, and E. Jondeau, "Experimental Investigation on the Fluctuation Intensities in a Stationary Spray," SAE Paper, 981066, 1998.

[32] R. Payri, J. M. García, F. J. Salvador, and J. Gimeno, "Using spray momentum flux measurements to understand the influence of diesel nozzle geometry on spray characteristics," *Fuel*, vol. 84, no. 5, pp. 551–561, 2005.

[33] I. V. Roisman, L. Araneo, and C. Tropea, "Effect of ambient pressure on penetration of a diesel spray," *International Journal of Multiphase Flow*, vol. 33, no. 8, pp. 904–920, 2007.

[34] J. Benajes, S. Molina, C. González, and R. Donde, "The role of nozzle convergence in diesel combustion," *Fuel*, vol. 87, no. 10-11, pp. 1849–1858, 2008.

[35] W. H. Nurick, "Orifice cavitation and its effect on spray mixing," *Journal of Fluids Engineering, Transactions of the ASME*, vol. 98, no. 4, pp. 681–687, 1976.

[36] F. Payri, V. Bermúdez, R. Payri, and F. J. Salvador, "The influence of cavitation on the internal flow and the spray characteristics in diesel injection nozzles," *Fuel*, vol. 83, no. 4-5, pp. 419–431, 2004.

[37] R. Payri, F. J. Salvador, J. Gimeno, and J. de la Morena, "Effects of nozzle geometry on direct injection diesel engine combustion process," *Applied Thermal Engineering*, vol. 29, no. 10, pp. 2051–2060, 2009.

[38] S. K. Aggarwal, "A review of spray ignition phenomena: present status and future research," *Progress in Energy and Combustion Science*, vol. 24, no. 6, pp. 565–600, 1998.

[39] F. Pischinger, U. Reuter, and E. Scheid, "Self ignition of diesel sprays and its dependence on fuel properties and injection parameters," *Journal of Engineering for Gas Turbines and Power*, vol. 110, no. 3, pp. 399–404, 1988.

[40] J. M. Desantes, J. V. Pastor, and S. A. Molina, "Analysis of the combustion process in a heavy duty D.I. diesel engine through in-cylinder visualisation," ICE, pp. 105–113, 1999.

[41] J. E. Dec, "A Conceptual Model of D.I. Diesel Combustion Based on Laser-Sheet Imaging," SAE Paper 970873, 1997.

[42] J. E. Dec and C. Espey, "Chemiluminescence Imaging of Autoignition in a DI Diesel Engine," SAE Paper, 982685, 1998.

[43] H. Hiroyasu, "Diesel engine combustion and its modeling," in *Proceedings of the International Symposium on Diagnostics and Modeling of Combustion in Reciprocating Engines*, pp. 53–75, 1985.

[44] C. Alıgrot, J. C. Champoussın, N. Guerassı, and G. Claus, "A correlative model to predict autoignition delay of diesel fuels," SAE Paper, 970638, 1997.

[45] D. N. Assanis, Z. S. Filipi, S. B. Fiveland, and M. Syrimis, "A predictive ignition delay correlation under steady-state and transient operation of a direct injection diesel engine," *Journal of Engineering for Gas Turbines and Power*, vol. 125, no. 2, pp. 450–457, 2003.

[46] H. Fujimoto, T. Shimada, and G. Sato, "Study of diesel combustion in a constant volume vessel," *Transactions of the Japan Society of Mechanical Engineers*, vol. 45, no. 392, pp. 599–609, 1979.

[47] G. S. Settles, *Schlieren and Shadowgraph Techniques: Visualizing Phenomena in Transparent Media*, Springer, New York, NY, USA, 2001.

[48] V. Macián, V. Bermúdez, R. Payri, and J. Gimeno, "New technique for determination of internal geometry of a diesel nozzle with the use of silicone methodology," *Experimental Techniques*, vol. 27, no. 2, pp. 39–43, 2003.

[49] H. Chaves, M. Knapp, A. Kubitzek, F. Obermeier, and T. Schneider, "Experimental study of cavitation in the nozzle hole of diesel injectors using transparent nozzles," SAE Paper, 950290, 1995.

[50] C. Bae, J. Yu, J. Kang, J. Kong, and K. O. Lee, "Effect of Nozzle Geometry on the Common-Rail Diesel Spray," SAE Paper, 2002-01-1625, 2002.